A Direct Methodology for Prediction of Creep Life Based on Small Punch Creep Test

Taeksang Lee

The Graduate School
Sungkyunkwan University
Department of Mechanical Engineering

A Direct Methodology for Prediction of Creep Life Based on Small Punch Creep Test

Taeksang Lee

The Graduate School
Sungkyunkwan University
Department of Mechanical Engineering

A Direct Methodology for Prediction of Creep Life Based on Small Punch Creep Test

Taeksang Lee

A Master's Thesis Submitted to the Department of Mechanical Engineering
and the Graduate School of Sungkyunkwan University
in partial fulfillment of the requirements
for the degree of Master of Science in Engineering

October 2015

Approved by
Moon Ki Kim
Major Advisor

This certifies that the master's thesis
of Taeksang Lee is approved.

Thesis Supervisor: Moon Ki Kim

Thesis Committee Chairman: Jae-Boong Choi

Thesis Committee Member: Kyunghoon Kim

The Graduate School
Sungkyunkwan University
December 2015

Contents

List of Tables

List of Figures

Summary

A Direct Methodology for Prediction of Creep Life Based on Small Punch Creep Test

Small punch creep test (SPCT) is a method to evaluate creep properties of metallic material instead of uniaxial creep test which is a conventional creep test method. SPCT shows practical advantages compared with the traditional uniaxial creep test since a small sheet specimen ($10 \times 10 \times 0.5$ mm) can be obtained from in-service facilities or mechanical parts without damage. In addition, relatively shorter rupture time in SPCT is another merit. SPCT results, however, cannot be directly used because stress state of an SPCT specimen during deformation is not uniaxial stress state. In other words, a complicated stress state of the SPCT specimen prevents not only comparison with uniaxial creep test but also registration to a standard creep methodology. In order to overcome the obstacle, a novel methodology is suggested to directly analyze SPCT results in consideration of Chakrabarty's membrane stretching theory, which provides strain and stress analysis on thin sheet material forced by large punch ball, and it is applied to derive von-Mises equivalent strain and strain rate from thickness change of the specimen. Therefore, general creep curves can be plotted only by using SPCT results. Furthermore, the Monkman-Grant model, which is an extrapolation method for evaluation of creep life, is investigated by using von-Mises equivalent strain and strain rate data calculated from the Chakrabarty's membrane stretching theory. To verify this methodology, both SPCT and uniaxial creep test results of STS 316L at 650℃ are used.

Displacement and time data in SPCT were converted into von-Mises equivalent strain and strain rate. The Monkman-Grant models derived from two different creep tests show a great potential such that SPCT with the proposed methodology can be substituted for uniaxial creep test.

Keywords: Small Punch Creep Test, Membrane stretching theory, Creep life expectation, Monkman-Grant model, STS 316L

1 Introduction

1.1 Background

Recently, most of countries have great concern about how to maximize energy efficiency due to not only their official duty to reduce carbon dioxide emission but also disappointing return on investment to renewable energy business. According to the International Energy Agency (IEA)'s report of the G8 Summit in 2008, operating efficiency of coal-fired power plants should be enhanced above 40% in order to reduce the amount of carbon dioxide emission and the volume of coal consumption [1]. Since Korea is also a member of the IEA, many Korean engineers focus on how to enhance operating efficiency of coal-fired power plants, and, as a result, that is increased like Figure 1.1. If the temperature of main steam in coal-fired power plant increases by 20℃, thermal efficiency will also increase up to about 1%.

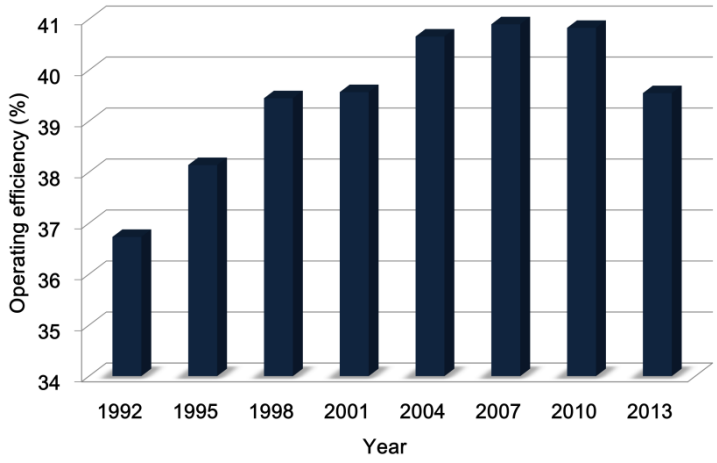

Figure 1.1 Change of operating efficiency of Korean coal-fired power plant during past decades

However, inherent creep property of metallic materials is the principal obstacle which prevents improvement of operating efficiency. In general, metallic materials at temperature above a half of their melting temperature on absolute scale show significant creep deformation which cannot be explained by mechanical properties at room temperature. In any facilities or mechanical components operated at high temperature, therefore, creep deformation must be taken into account critically. Thanks to many great senior researchers, experiment methods and microscopic analyses on creep issues have been well studied, and especially uniaxial creep test, suggested by ASTM E139-11 [2], has been used to obtain creep properties of metallic material universally. However, as uniaxial creep test needs bulk of materials, this test cannot be applied to in-service facilities or components for real-time monitoring on creep deformation.

To overcome this limitation, Small Punch Creep Test (SPCT) has been alternatively suggested to evaluate creep properties of in-service material [3, 4]. Since SPCT just needs a thin sheet of material (10×10×0.5 mm), it is well fitted to determine creep properties of in-service components at high temperature without damage. Furthermore, SPCT has an advantage in test time because rupture in SPCT happens very quickly compared to the conventional uniaxial creep test.

Although SPCT shows strong advantages and potentials, it does not become a standard creep test method like uniaxial creep test. This is because stress state of SPCT is very different with that of uniaxial creep test, and therefore a direct comparison between SPCT and uniaxial creep test has not been possible. An SPCT specimen is deformed at multi axial stresses, while that of uniaxial creep test is deformed at a uniaxial stress. In other words, it is difficult to obtain a representative value of stress and strain in SPCT. For this reason, Finite Element (FE) analysis on

SPCT should be accompanied to derive equivalent stress and strain value, and those are simply compared with stress and strain in uniaxial creep test. This process, however, also results in another problem that data in other researcher's papers cannot be effectively cited since FE models from each researcher cannot be exactly same. Hence, fundamental and essential understanding on deformation mechanism of SPCT specimen is definitely needed to better use SPCT.

1.2 Previous study

Various studies on SPCT have been carried out during several decades. Chakrabarty [5] has suggested an analytical solution through membrane stretching theory. Although the author has investigated deformation characteristics of small punch test specimen at room temperature with a specific material and a perfect lubrication condition, the analytical solution is very practical even for SPCT at high temperature and used for various materials by other researchers. Yang and Wang [6] have provided an empirical relationship between strain and central deflection of SPCT specimen by using Chakrabarty's membrane stretching theory. Chen [7] has investigated non-dimensional analysis to obtain creep properties of material. Hyde [8] has developed general strain analysis using membrane stretching theory and FE method. Also, the European Committee for Standardization has carried out a Code of Practice for SPCT [9].

Furthermore, lots of researchers have studied on how to interpret SPCT results in order to compare with uniaxial creep test results [9-12]. Not only 2-dimensional or 3-dimensional FE models [13-16] have been developed to obtain local strain and stress data, but also microscopic analysis [17, 18] on specimen has validated creep phenomenon within an SPCT specimen. From these diverse studies, certain empirical equations about stress and strain of SPCT have been derived [9], and stress distribution on SPCT specimen in the process of experiment is revealed by FE analysis [19]. In addition, many studies on boundary conditions, factors, and parameters affecting SPCT results have been carried out [6, 13, 17].

To better understand a ruptured SPCT specimen, there have been several studies on a failure position. Park [17] has investigated thickness decrease of every position

on an SPCT specimen right before failure and compared it with FE analysis result. It has suggested that the thinnest point on a specimen is a dominant position to cause total failure of SPCT with the highest stress concentration. Other studies have also provided that rupture occurs near the thinnest point of the specimen and its location does not change during the test, and therefore investigation of the thinnest point has been carried out in order to obtain creep properties through FE analysis [7, 16, 17]. Especially, Lee's observation of fracture surface shows microscopic evidence such as growth and coalescence of crack at the thinnest point and occurrence of intergranular fracture caused by intergranular cavity crack at that point [18]. Lee's study not only provides creep deformation mechanism on SPCT specimen, but also explains why the thinnest point is important to procure creep properties from SPCT.

For more practical purpose, SPCT results have been applied to the Monkman-Grant model [20] which is a method to predict material's creep life. Lots of studies have suggested that SPCT has a possibility to build the Monkman-Grant model [21-25]. Besides, the Monkman-Grant model derived by SPCT has been compared with that derived by uniaxial creep test [10, 26]. Although above studies related to the Monkman-Grant model of SPCT have already shown the possibility to assess creep life, those are also insufficient because not only understanding on deformation mechanism of SPCT specimen is deficient, but also a correction factor between SPCT and uniaxial creep test is always required with respect to type of materials.

1.3 Objectives

It is obvious that SPCT has a strong potential for practical use to assess creep life of fossil fired power plant components in that SPCT specimen can be procured from in-service components without damage. To realize this advantage, SPCT must be an independent test method without uniaxial creep test result as well as FE analysis. In this regard, I suggest a direct methodology, which is based on an analytical solution in Chakrabarty's membrane stretching theory, for creep life prediction of material. Especially, I connect Chakrabarty's membrane stretching theory to the Monkman-Grant model.

Furthermore, how to procure creep properties such as equivalent strain and strain rate is also suggested in this paper. To be specific, Chakrabarty's membrane stretching theory is directly applied to SPCT results, and equivalent strain and strain rate diagrams of SPCT are illustrated from the analytical solution. Both uniaxial creep test and SPCT results using STS 316L at the test temperature of 650℃ [27, 28], which is operation condition in power plants, are cited to validate the proposed methodology.

Based on the results of equivalent strain analysis, the Monkman-Grant model for SPCT is derived, and that for uniaxial creep test is also obtained. I will show that the Monkman-Grant model of SPCT results is compatible with that of uniaxial creep test since dimensional problem is solved by equivalent strain analysis. Finally, comparison of the Monkman-Grant models provides a good correlation between uniaxial creep test and the direct methodology using SPCT results.

2 Theoretical background

2.1 Creep

Mechanical properties of most metallic materials at room temperature are independent of time. However, at elevated temperature, the mechanical properties become very dependent on both time and strain rate. If metallic materials are subjected to a static tensile load at above a half of melting temperature, T_m, on an absolute temperature scale, the metallic materials undergo a time-dependent deformation even below yield strength. This phenomenon is called creep and it is a critical issue in power plant where mechanical equipment such as boilers and steam turbines is operated with high temperature and pressure condition.

In order to investigate creep deformation of metallic materials, there are two general tests which are creep test and stress-rupture test. The creep test measures the amount of deformation which results from elevated temperature exposure and the stress-rupture test, on the other hand, assesses the effect of temperature on the load-bearing capability. For evaluation on creep characteristics of metallic materials, ASTM E139-11 [2] suggests a standard test method called a uniaxial creep test that a constant load is applied to a tensile specimen maintained at a constant temperature and the strain of the specimen is obtained with respect to time. The creep test is similar to the stress-rupture test in that both tests are performed by the uniaxial creep test. The former, however, is often carried out to less than 0.5 percent strain, while the latter is carried out to the failure of the material. Higher loads are used in the stress-rupture test than in the creep test, and hence the creep rates are higher.

Figure 2.1 shows the idealized creep curve at a constant load and there are three stages which are primary creep, secondary creep, and tertiary creep. Primary creep stage shows initial large and rapid strain, ε_0, including elastic and plastic deformation. Following initial strain ε_0, creep rate, $\frac{\mathrm{d}\varepsilon}{\mathrm{dt}}$, which is the slope of creep curve, is decreased continuously due to increase of creep resistance results from its own deformation. Then the creep rate reaches minimum value and becomes a steady state in which the creep rate changes little with respect to time. This is because work hardening speed by increase of dislocation density in material from plastic deformation is balanced with recovery speed by dynamic softening and local diffusion of atoms. Secondary creep stage occupies most of creep test as shown in Figure 2.1. Finally, tertiary creep stage shows sudden increase of creep rate and, after all, material is fractured with a reduction in cross-sectional area results from necking or void coalescence. If constant stress creep test is carried out, tertiary creep stage is delayed since effect of reduction in cross-sectional area is neglected. Most engineering components, however, are usually subjected to load not a constant stress and therefore constant load creep test is more practical [29]. And the initial stress applied to specimen is generally labeled for the value of stress.

Once creep curve is obtained like Figure 2.1, creep rate curve is also drawn as Figure 2.2 in which creep rate is plotted with respect to time. This curve shows dramatic change in creep rate and obvious division. From comparing Figure 2.2 with Figure 2.1, creep rate has a minimum value only in secondary creep stage. To determine minimum creep rate, $\dot{\varepsilon}_s$, in Figure 2.2, the average value of the creep rate during secondary creep is calculated and used.

In a range of metals, $\dot{\varepsilon}_s$ at temperature above $0.5T_m$ is simply formulated by a power law relation [29, 30]

$$\dot{\varepsilon}_s = B\sigma^n e^{-\frac{Q}{kT}} \tag{2.1.1}$$

Where B is a constant, σ is applied stress, Q is activation energy, k is Boltzmann's constant, and T is temperature on absolute scale. This power law relation can be used for both high and low temperature condition.

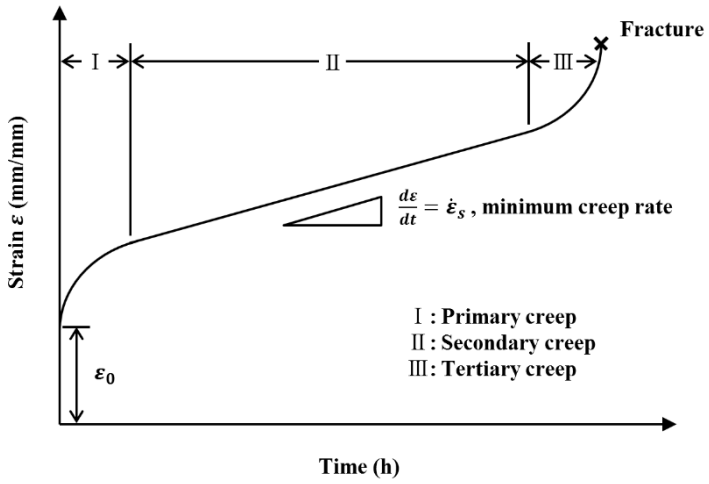

Figure 2.1 General creep curve with a constant load

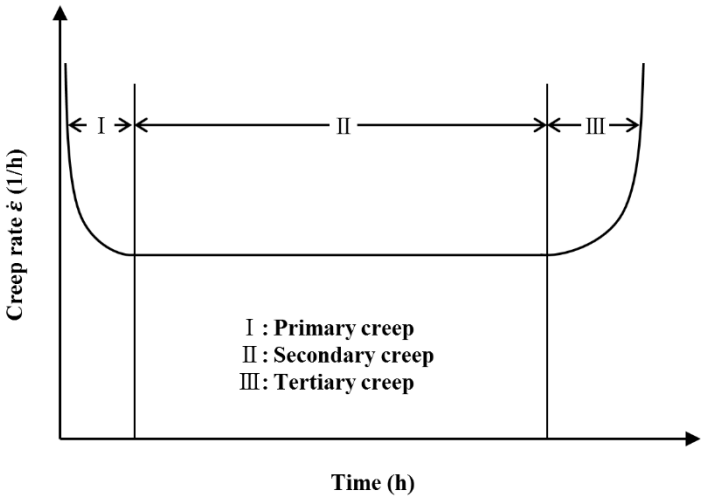

Figure 2.2 Creep rate curve with respect to time

2.2 Creep mechanism

Since applied stress and temperature are constant, time-dependent creep deformation results from metallurgical changes in material. Solid state diffusion results from thermal activation and slip or glide processes of plastic deformation are dominant factors to yield creep deformation. If temperature is high enough, diffusion is a dominant mechanism of creep deformation, while if temperature is relatively low, slip or glide processes are a dominant mechanism of creep deformation. Hence, according to the prevailing temperature and stress, creep mechanisms can be divided in deformation mechanism map in which x-axis means homologous temperature, $\frac{T}{T_m}$, and y-axis has normalized shear stress, $\frac{\sigma}{G}$, where G is shear modulus [31, 32]. Based on deformation mechanism map, creep mechanisms are mainly classified as dislocation creep, dislocation glide creep, and diffusion creep [29].

Dislocation creep occurs at relatively high stress and temperature, and diffusion of vacancies or interstitials assists movement of dislocation so that dislocation overcomes barriers [31, 32].

Dislocation glide creep occurs at much higher stress and lower temperature than those ordinarily expected to yield creep deformation [33]. Thermal activation helps dislocation move along slip planes and overcome obstacles, and therefore material is deformed [29].

Diffusion creep is prevalent at high temperature and relatively low stress in deformation mechanism map. Depending on stress level, diffusion creep is group as Nabarro-Herring creep, Coble creep, and Harper-Dorn creep. Firstly, Nabarro [34] and Herring [35] suggested that creep at high temperature and low stress was controlled by atomic diffusion in bulk, and creep rate was formulated as:

$$\dot{\varepsilon}_s = \frac{A_{NH}\sigma D_l \Omega}{kTd^2} \quad (2.2.1)$$

Where A_{NH} is a geometric constant, D_l is lattice diffusion coefficient, Ω is vacancy volume, and d is grain diameter. Second, at lower temperature, grain boundary diffusion is dominant in material and creep rate is represented by Coble [36] as:

$$\dot{\varepsilon}_s = \frac{A_c \sigma D_{gb} \delta \Omega}{kTd^3} \quad (2.2.2)$$

Where A_c is a geometric constant, D_{gb} is grain boundary diffusion coefficient, and δ is grain boundary width. Coble creep does not maintain if grain boundary sliding does not occur simultaneously [29, 37]. Lastly, at relatively low stress, diffusion assisted by dislocation climb can be a determinant of creep rate [38, 39]. Harper and Dorn provided relation of creep rate like:

$$\dot{\varepsilon}_s = \frac{A_{HD}\sigma D_l b}{kT} \quad (2.2.3)$$

Where A_{HD} is a constant and b is Burgers vector of the dislocation.

2.3 Membrane stretching theory

Chakrabarty's study provided a general analytical solution on plastic deformation of stretching forming over hemispherical punch heads, and the analytical solution with selective materials under perfect lubrication assumption between the punch and material showed a good agreement with experimental results [5, 40]. Figure 2.3 shows a spherical pressure vessel in a spherical coordinate and represents the stress state of an infinitesimal element and Figure 2.4 shows a schematic of Chakrabarty's membrane stretching model in 2-dimensional cross section view including z-axis in Figure 2.3.

In Figure 2.3, the spherical pressure vessel forms a surface of revolution with respect to z-axis and the element, which has a thickness, *t*, is defined by spherical coordinate system. Radial direction component is *R*, circumferential direction is θ and meridional direction is ϕ. The stress state of the element is also represented by spherical coordinate system and the component of the stress state shows radial stress, *p*, in radial direction, circumferential stress, σ_θ, in θ direction and meridional stress, σ_ϕ, in ϕ direction. Basically, when the element is located apart from *r*, which is a vertical distance from z-axis, the circumferential and meridional radii of curvature are formulated like:

$$\rho_\theta = r\,\mathrm{cosec}\,\phi\,,\ \rho_\phi = \frac{\partial r}{\partial \phi}\sec\phi \tag{2.3.1}$$

ρ_θ is the circumferential radius of curvature and ρ_ϕ is the meridional radius of curvature. And due to exact spherical shape, ρ_θ and ρ_ϕ should be defined like:

$$\rho_\theta = \rho_\phi = R \tag{2.3.2}$$

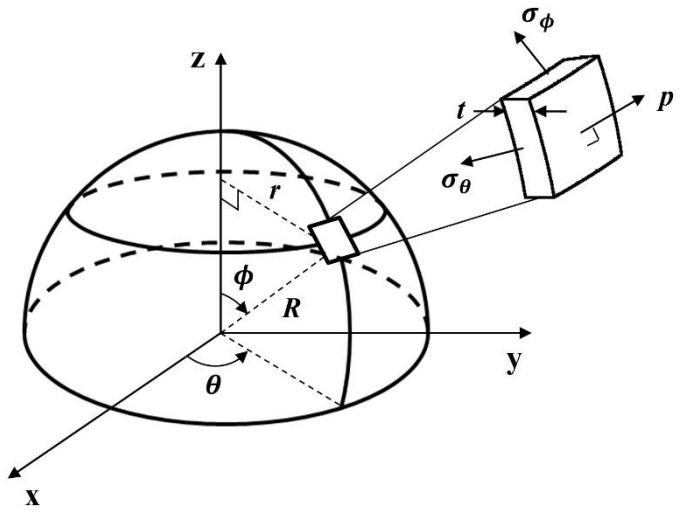

Figure 2.3 Spherical coordinate for hemispherical pressured vessel

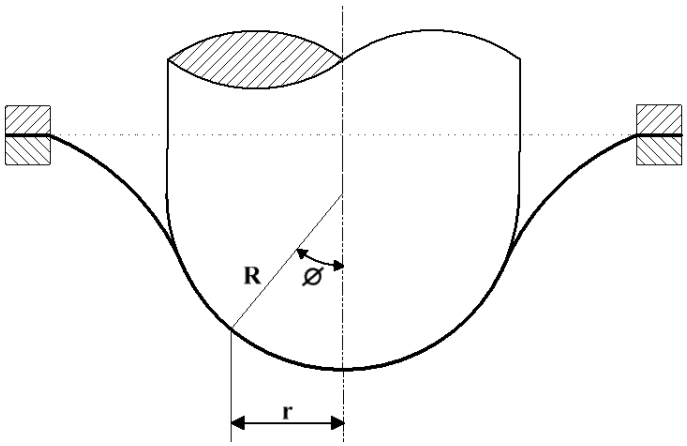

Figure 2.4 A schematic of Chakrabarty's membrane stretching model in SPCT

In order to derive the meridional equilibrium equation, meridional components of the circumferential and meridional stress are used. The meridional components of meridional and circumferential stress are as follows, respectively,

$$\left(\sigma_\phi trd\theta\right)\cos\frac{d\phi}{2}-\left\{\left(\sigma_\phi trd\theta\right)+\frac{\partial(\sigma_\phi trd\theta)}{\partial r}dr\right\}\cos\frac{d\phi}{2} \tag{2.3.3}$$

$$(\sigma_\theta tRd\phi)\sin\frac{d\theta}{2}\sin(\frac{\pi}{2}-(\phi+\frac{d\phi}{2}))+\left\{(\sigma_\theta tRd\phi)+\frac{\partial(\sigma_\theta tRd\phi)}{\partial\theta}d\theta\right\}\sin\frac{d\theta}{2}\sin(\frac{\pi}{2}-(\phi+\frac{d\phi}{2})) \tag{2.3.4}$$

Figure 2.5 (a) shows all stress components of infinitesimal element on the spherical thin vessel, and Figure 2.5 (b) and (c) show direction of meridional stress and circumferential stress, respectively. As geometric condition, which is exactly spherical, R and r have the relationship like equation. 2.3.1 and 2.3.2. Also, for small angle of $d\phi$ and $d\theta$, $\sin\frac{d\phi}{2}$ and $\sin\frac{d\theta}{2}$ can be approximated to $\frac{d\phi}{2}$ and $\frac{d\theta}{2}$. Likewise, $\cos\frac{d\phi}{2}$ and $\cos\frac{d\theta}{2}$ are to be 0. Each stress component is tilted by $\frac{d\phi}{2}$ and $\frac{d\theta}{2}$, respectively, as shown in Figure 2.5. The meridional stress is tilted by $\frac{d\phi}{2}$ to the meridional direction while the circumferential stress is tiled by $\frac{d\theta}{2}$ to the circumferential direction due to the curvature. Summation of equation 2.3.3 and 2.3.4 is equal to 0 because the element is in stress equilibrium state and, thus, the result of summation is like:

$$\frac{\partial}{\partial r}\left(t\sigma_\phi\right)=\frac{t}{r}\left(\sigma_\theta-\sigma_\phi\right) \tag{2.3.5}$$

Normal equilibrium can be simply derived by manipulating of equation 2.3.3 and 2.3.4 because meridional direction is vertical to the normal direction, which is p

direction. The normal component of meridional and circumferential stress is respectively as:

$$\left(\sigma_\phi trd\theta\right)\sin\frac{d\phi}{2}-\left\{\left(\sigma_\phi trd\theta\right)+\frac{\partial(\sigma_\phi trd\theta)}{\partial r}dr\right\}\sin\frac{d\phi}{2} \tag{2.3.6}$$

$$(\sigma_\theta tRd\phi)\sin\frac{d\theta}{2}\cos(\frac{\pi}{2}-(\phi+\frac{d\phi}{2}))+\left\{(\sigma_\theta tRd\phi)+\frac{\partial(\sigma_\theta tRd\phi)}{\partial\theta}d\theta\right\}\sin\frac{d\theta}{2}\cos(\frac{\pi}{2}-(\phi+\frac{d\phi}{2})) \tag{2.3.7}$$

Summation of equation 2.3.6 and 2.3.7 is equal to $pd\phi Rd\theta r$ and thus, the normal equilibrium is like:

$$p=\frac{t}{R}(\sigma_\theta+\sigma_\phi) \tag{2.3.8}$$

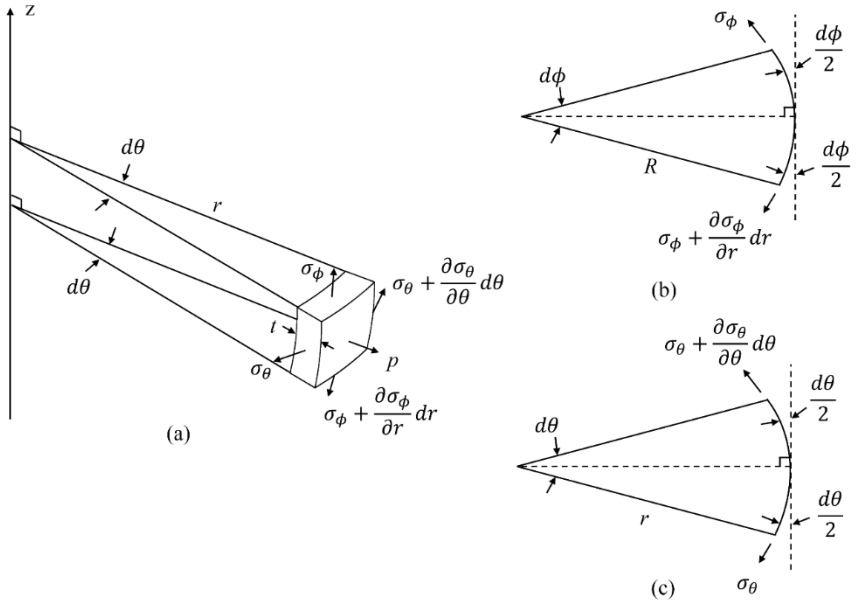

Figure 2.5 Stress state of infinitesimal element on the spherical thin vessel: (a) All stress components; (b) Meridional stress; and (c) Circumferential stress

2.4 von-Mises equivalent strain

Based on Chakrabarty's membrane stretching theory [5], the element undergoes only three normal stresses since a material is assumed to be perfectly lubricated. Therefore, the state of the material is principal stress state and each current stress direction means the principal direction of stress for that element. And a material is postulated to experience ideally plastic deformation with a constant yield stress in accordance with Levy-Mises flow rule [5, 40], in which elastic deformation is neglected since it is relatively very small. Also, Poisson's ratio of material is set to be 0.5 in incompressible condition and the principal direction of stress is assumed to be equal to direction of strain increment or strain rate. Hence, incompressible condition can be expressed such that

$$\varepsilon_{kk} = J_1 = 3\varepsilon_m = \varepsilon_{11} + \varepsilon_{22} + \varepsilon_{33} = \varepsilon_\theta + \varepsilon_\phi + \varepsilon_t = 0 \tag{2.4.1}$$

$$\varepsilon'_{ij} = \varepsilon_{ij} - \varepsilon_m \delta_{ij} = \varepsilon_{ij} \tag{2.4.2}$$

In this case, the first plastic strain invariant, J_1, is 0 and thus, the deviatoric strain tensor, ε'_{ij}, is equal to the plastic strain tensor, ε_{ij}, since the mean strain, ε_m, is also 0. ε_θ, ε_ϕ, ε_t, and δ_{ij} mean the circumferential strain, meridional strain, radial strain which is direction of thickness, and Kronecker delta, respectively. Each strain term means the principal strain as well.

True strain calculation is derived as logarithmic expression,

$$\int_{l_0}^{l} \frac{dx}{x} = \ln \frac{l}{l_0} \tag{2.4.3}$$

Where l_0 and l is the initial and final length, respectively. If r_0 is initial position of the element which is located apart from r, ε_θ can be considered change of hoop circumference like:

$$\varepsilon_\theta = \ln\frac{2\pi r}{2\pi r_0} = \ln\left(\frac{r}{r_0}\right) \tag{2.4.4}$$

Likewise, ε_ϕ is regarded as that initial length dr_0 is changed to $dr\sec\phi$. ε_t is also simply calculated by thickness change, t_0 to t.

$$\varepsilon_\phi = \ln\left(\frac{\partial r}{\partial r_0}\sec\phi\right), \quad \varepsilon_t = \ln(\frac{t}{t_0}) \tag{2.4.5}$$

Biaxial tension on the element provides $\sigma_\theta = \sigma_\phi$ and therefore, ε_θ is also equal to ε_ϕ. From this relationship, the von-Mises equivalent strain, ε_q, is represented as:

$$\varepsilon_q = \sqrt{\frac{2}{3}\varepsilon'_{ij}\varepsilon'_{ij}} = \sqrt{\frac{2}{3}\varepsilon_{ij}\varepsilon_{ij}} = \sqrt{\frac{2}{3}({\varepsilon_\theta}^2 + {\varepsilon_\phi}^2 + {\varepsilon_t}^2)} = |\varepsilon_t| = ln(\frac{t_0}{t}) \tag{2.4.6}$$

Hence, the von-Mises equivalent strain can be obtained directly by measuring the thickness of a specimen.

2.5 Monkman-Grant model

The Monkman-Grant model, a method to predict the creep life of metallic material, is composed of the creep failure time t_f, minimum creep rate $\dot{\varepsilon}_s$, and constants *m* and *C* such that

$$t_f \dot{\varepsilon}_s{}^m = C \tag{2.5.1}$$

Depending on metals, the constant *m* varies between 0.8 and 0.95, while the constant *C* varies between 3 and 20 when t_f has unit of hour and $\dot{\varepsilon}_s$ has unit of percent over hour respectively [20]. It is also reported that the constant *m* depends on the microstructure of material such as grain size [41]. In general, equation 2.5.1 is used after it is converted into logarithmic scale. After conversion, it is plotted as a straight linear graph, which has *m* slope. Using this linear graph, long term creep life can be expected by using linear approximation. In this paper, the Monkman-Grant models of uniaxial creep test and SPCT are examined and compared to each other. The results of SPCT mostly have a shorter rupture time rather than those of uniaxial creep test in the Monkman-Grant model.

3 Experimental procedure

3.1 Material and specimen

STS 316L, which is an austenite type stainless steel, is widely used in fossil and atomic power plant since it is representative steel including good heat-resistant property. “L” in the word of STS 316L means low carbon content in the material and, therefore, STS 316L does not suffer from intergranular corrosion since carbon plays a strong role to reduce the resistance to intergranular corrosion resulted from carbide formation [42]. Melting temperature of STS 316L is 1375 to 1400℃ [43] and specific compositions of STS 316L are shown in Table 3.1.

Table 3.1 Chemical compositions of STS 316L [28]

C	Si	Mn	P	S	Ni	Cr	Mo	Fe
0.02	0.62	0.69	0.021	0.002	12.23	17.37	2.16	Bal.

A uniaxial creep test needs round bar shaped specimen with the gage section diameter of 6 mm and gage length of 30 mm as shown in Figure 3.1 (a). In contrast, as shown in Figure 3.1 (b), SPCT needs a very thin sheet specimen ($10 \times 10 \times 0.5$ mm), which is much smaller than a typical uniaxial creep specimen. Better comparison between uniaxial creep specimen and SPCT specimen is depicted in Figure 3.2. One uniaxial creep specimen requires material for more than two hundreds of SPCT specimens.

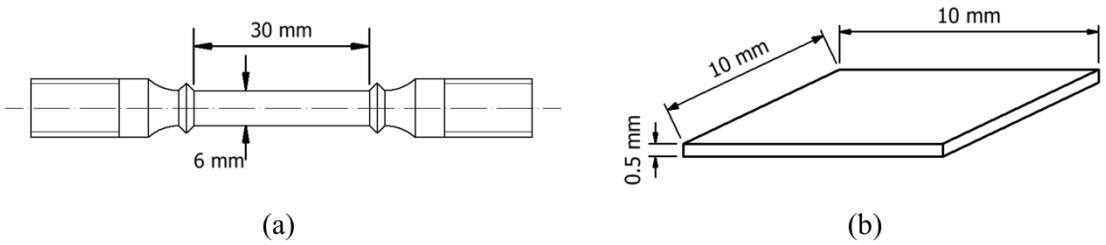

Figure 3.1 Type of creep test specimen: (a) Uniaxial creep test and (b) SPCT [44]

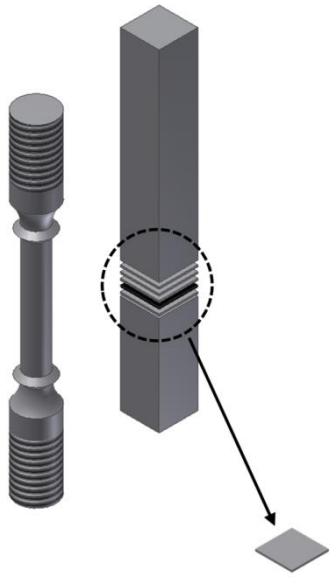

Figure 3.2 Comparison between uniaxial creep specimen and SPCT specimen [44]

3.2 Test equipment

Both 2-D and 3-D Schematics of an SPCT tester are shown in Figure 3.3. R is a radius of punch ball (1.2 mm), a is an inner radius of lower die (2 mm), b is a fillet radius (0.2 mm) of lower die, and t_0 is an initial thickness of specimen (0.5 mm). As shown in Figure 3.3 (a), each central vertical axis of punch, punch ball and specimen should coincide with one another in order to avoid anisotropic effect. In other words, punch ball should convey force through the exact center point of specimen and then eventually penetrate it. Hence, t_0 has to be uniform in order to prevent deviation of force direction. To make a flat specimen with a constant thickness, every SPCT specimen is polished by coarse to micro fine polishing paper. Also, the surface of specimen must be flawless. This is the reason why SPCT is normally performed in argon gas condition to prevent oxidation. The upper and the lower die also play an important role in hampering slip between specimen and punch ball. Without appropriate force transmission, membrane stretching theory cannot be applied to SPCT. Thus, each test should accompany all the above requirements. Overall picture of SPCT equipment is like Figure 3.4 and 3.5 which are for constant and dynamic load condition, respectively. The equipment in Figure 3.4 can perform SPCT only, while the tester in Figure 3.5 is able to carry out small punch test at room temperature as well as high temperature. And both testing machines measure punch displacement recorded by a linear variable differential transformer (LVDT) which has the capacity to measure the change of 1 μm.

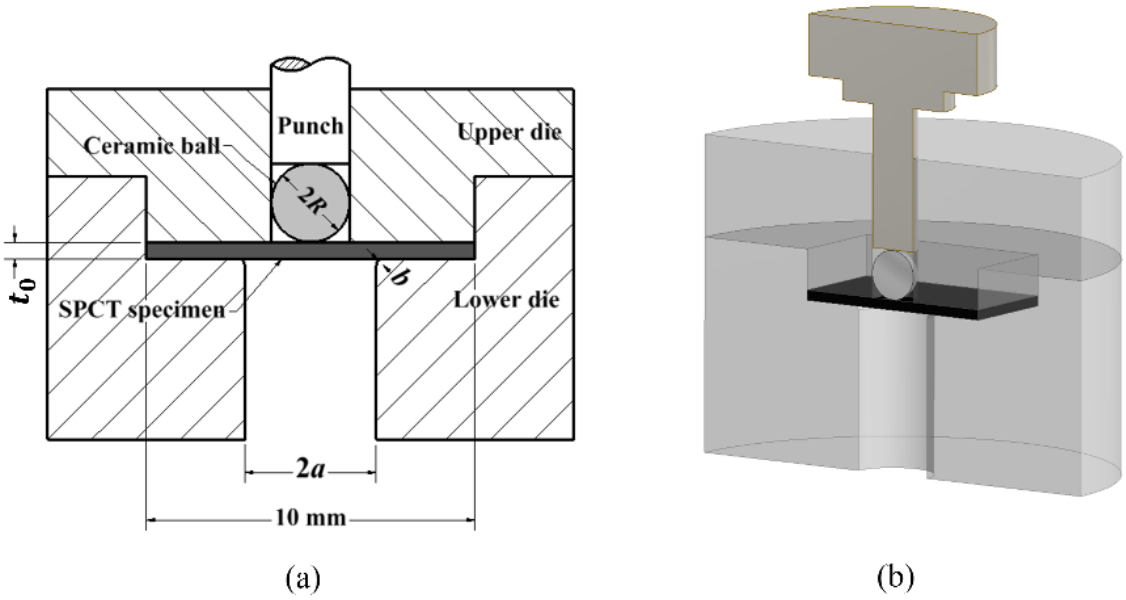

Figure 3.3 Schematics of SPCT: (a) 2-D model and (b) 3-D model [44]

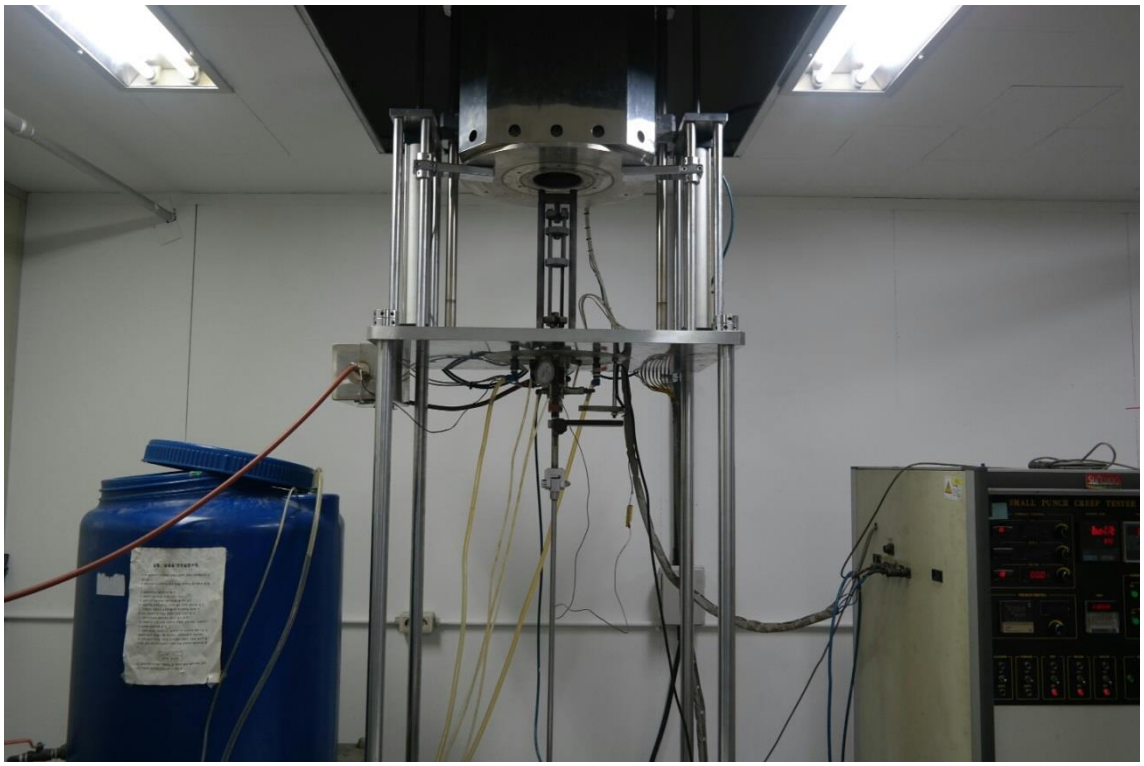

Figure 3.4 SPCT equipment for constant load condition

Figure 3.5 Small punch tester for dynamic load condition

3.3 Experimental method

3.3.1 SPCT

SPCT specimen is polished to be flat and have an initial thickness of 0.5 mm. Then, the specimen is placed between the upper and lower die in chamber which is with argon gas. This condition is to prevent oxidation of specimen. Temperature in the chamber is increased up to an objective temperature, and a punch ball is loaded on the specimen once it reaches to a test temperature. Punch displacement is measured by an LVDT with respect to time.

Kim [28] has carried out SPCT for STS 316L at 650℃, homologous temperature $\frac{T}{T_m}$ is about 0.5, by using two different punch balls which are Si_3N_4 punch ball and Al_2O_3 punch ball. The author has experimented with four different loading conditions such as 421.83, 470.88, 549.36 and 598.41 N and investigated friction effect of punch ball. In this paper, Kim's results are cited for equivalent strain analysis.

3.3.2 Small punch test

General equipment and process of small punch test are mostly same with SPCT except loading and temperature condition. Small punch test is carried out at a dynamic load, while SPCT is performed at a constant load. Also, small punch test is conducted at room temperature, whereas SPCT is continued at temperature above $0.5T_m$.

To generate dynamic load, a servo motor, which is top part in Figure 3.5, controls displacement or load. In this study, punch displacement is regulated to 0.5 mm/min and measured by an LVDT likewise.

3.3.3 Thickness measurement

Once SPCT is carried out at certain test condition, a variation of punch displacement with respect to time is also obtained. Based on the punch displacement, each SPCT is interrupted to measure the least thickness of specimen at prescribed interval as shown in Figure 3.6, and this process is repeated until rupture. To be specific, center position of each stopped specimen is cut by a diamond cutting machine, and the half of specimen is treated by hot mounting process. Then, the least thickness is measured by optical micro scope. From this investigation, thickness value with respect to punch displacement can be procured.

Mao [45] has carried out small punch test using seven different materials which are HT-60, HT-9, 9Cr, A533B, A508, Cu-Be-Co, and STS 304. Especially, the author has investigated thickness change at the local necking and crack initiation position. He has also reported that loading capacity of the specimen is deteriorated by significant decrease of thickness and the circumferential crack propagation. In this paper, Mao's results are cited for equivalent strain analysis.

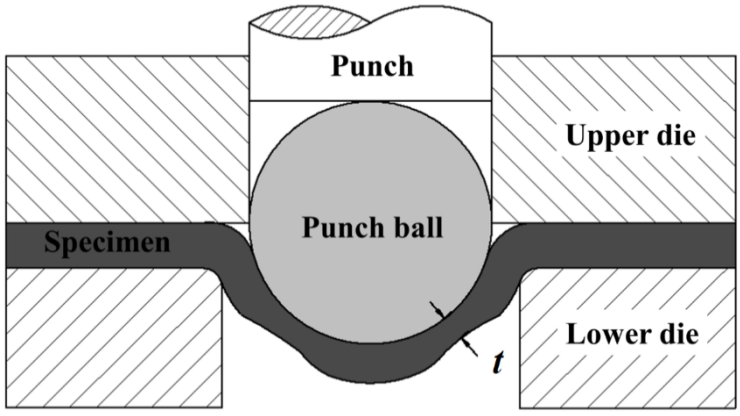

Figure 3.6 Measurement of thickness at the thinnest point [45]

4 Experimental results

4.1 Small punch test results

Small punch test is carried out by using STS 316L at room temperature, and applied load and punch displacement are recorded like Figure 4.1. Data is saved until fracture occurs like Figure 4.2. General graph of small punch test shows elastic, elastic and plastic, plastic deformation, and final failure [46]. Roughly speaking, a region near about 0.5 mm of punch displacement, which means the initial thickness of the specimen, is a transition from elastic to pure plastic as well as bending to membrane stretching deformation [45, 46]. Above separations of deformation features are based on shape of curve, and therefore each curve should be investigated carefully.

To be specific, the transition from bending to membrane stretching is elucidated both theoretically and experimentally. Chakrabarty [47] has provided an analytical solution on membrane stretching deformation as well as bending deformation, and he has suggested that membrane stretching deformation is dominant when punch displacement exceeds the initial thickness of specimen.

Figure 4.1 also shows a general curve of small punch test, and thus the perfect plastic deformation seems to occur after about 0.75 mm of punch displacement. In other words, the equivalent strain analysis in which the perfect plastic deformation is an assumption can be carried out after about 0.75 mm of punch displacement. Based on this information, data of SPCT above 0.75 mm of punch displacement is used to derive strain value in “equivalent strain analysis” section.

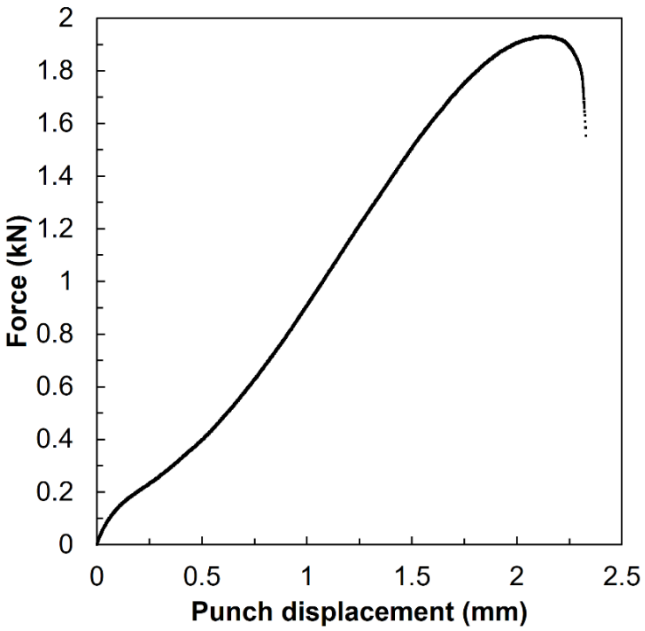

Figure 4.1 Small punch test result of STS 316L under 0.5 mm/min displacement control at room temperature

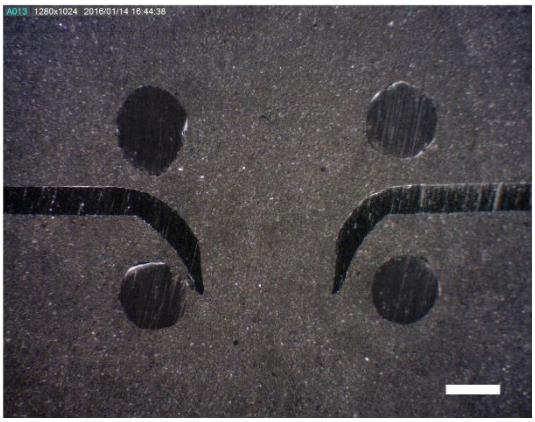

Figure 4.2 Cross sectional view of a fractured small punch test specimen. Scale bar, 1 mm

4.2 SPCT results

4.2.1 SPCT curves [28]

Figure 4.3 [28] represents SPCT curves, which show variation of punch displacement with respect to time, for STS 316L at 650℃ and, especially, the SPCT is carried out using different punch balls, one is Si_3N_4 and the other is Al_2O_3. Punch displacement is recorded until a punch ball passes completely through the specimen like Figure 4.4. Rupture in the specimen occurs along circumferential direction with respect to the punch ball movement, and feature of necking at the rupture position is also shown with the naked eye. An intensive decrease of thickness at certain position is directly used for equivalent strain analysis.

Kim [28] has investigated effect of friction of two different punch balls and showed that the difference of friction coefficient affects minimum punch displacement rate $\dot{h}$ and failure time t_f as shown in Figure 4.3. Also, the author determined that Si_3N_4 and Al_2O_3 have the friction coefficient, 0.5 and 0.4, respectively [28]. Although $\dot{h}$ and t_f vary depending on the type of punch ball, very typical creep behaviors consisting of initial rise, steady state increase, and rupture with necking are observed in both cases. These two different SPCT results are used to validate equivalent strain analysis, and the effect of friction coefficient of punch ball is discussed when creep life expectation is carried out.

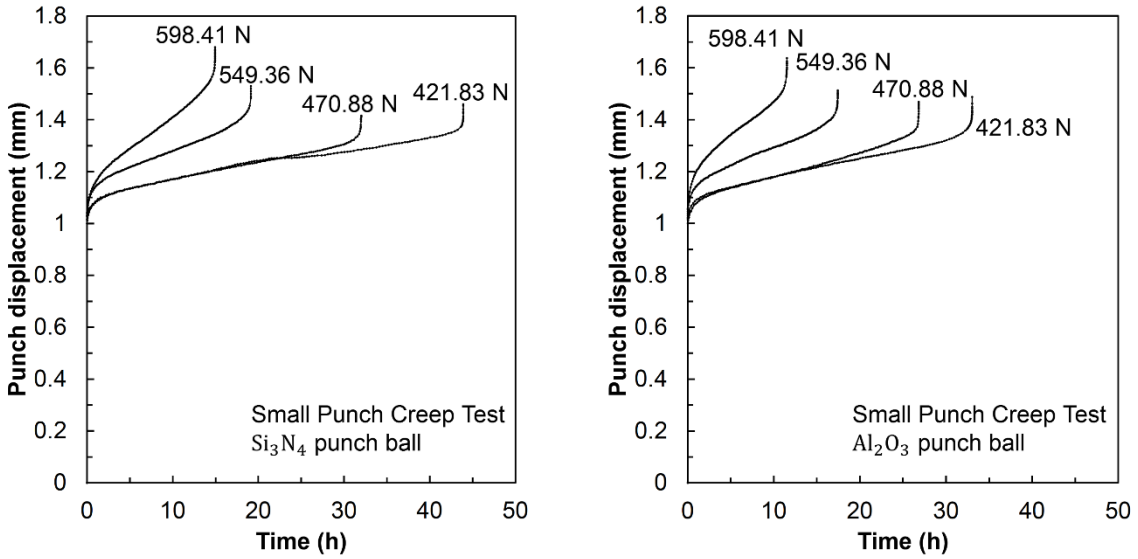

Figure 4.3 SPCT curves of STS 316L at 650℃: (a) Si_3N_4 punch ball and (b) Al_2O_3 punch ball [28]

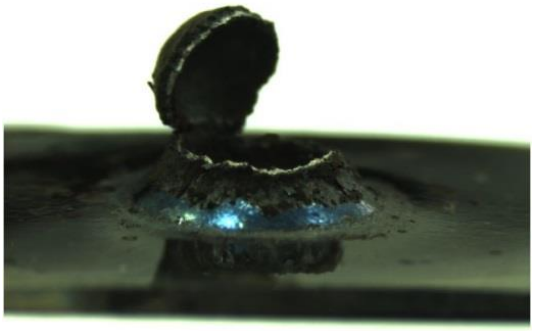

Figure 4.4 A ruptured SPCT specimen at 706.32 N and 650℃

4.2.2 Thickness change observation

Thickness change can be directly measured at the least thickness position. To do this study, interrupted SPCT specimens are investigated by using an optical microscope as shown in Figure 4.5. To be specific, SPCT is carried out at 706.32 N and 650℃. Each SPCT specimen is stopped when punch displacement is 1.12, 1.22, 1.26, 1.36, and 1.41 mm, respectively. Cross section of the specimen with solidified hot mounting resin not only facilitates work of the measurement of thickness, but also enhances accuracy of the measurement. In Figure 4.5, it is obvious that thickness of certain location is significantly decreased even though I myself do not conduct to measure the thickness. Hence, the least thickness position is not only a main deformation position but also a principal place in which creep rupture occurs.

In this paper, Mao's results [45] are cited for equivalent strain analysis. This is because Mao's results have been developed by various materials including stainless steel, and therefore I suppose that his results are reliable and suitable for a general application and validation of equivalent strain analysis. Furthermore, my experimental dimensions in SPCT are exactly same with Mao's that. From thickness change investigation at thinnest point, Mao [45] suggested an empirical equation of thickness t as a function of punch displacement h and the thickness t such that

$$\frac{t}{t_0} = e^{-1.2(\frac{h}{2})^{1.5}} \tag{4.2.1}$$

Note that this is only valid when experimental conditions such as dimension of specimen, punch ball size, and inner diameter of lower die are identical to Mao's experiment.

Even though Mao's empirical equation is derived from small punch test at room temperature not SPCT at high temperature, I assume that the change of the least thickness in a specimen is little different in both small punch test and SPCT since each specimen is strongly constrained until rupture. In other words, if boundary conditions in both tests are same, the deformation aspect would be little different. Based on this assumption, I have directly used equation 4.2.1 in equivalent strain analysis.

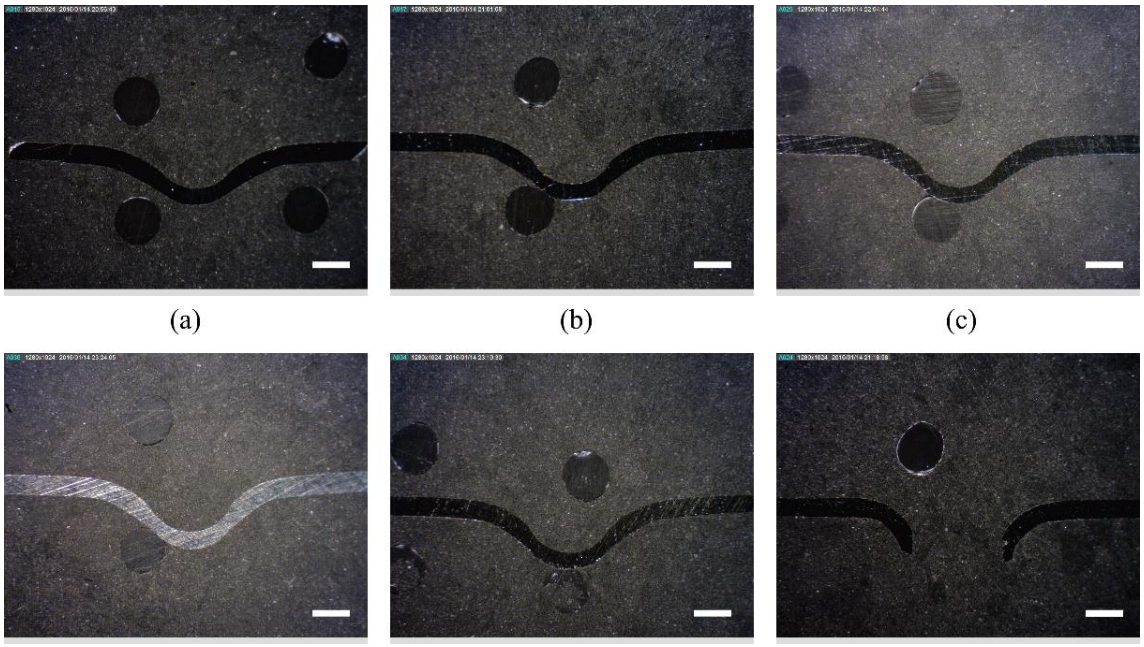

(a) (b) (c)

(d) (e) (f)

Figure 4.5 Cross sectional image of interrupted specimen with respect to punch displacement: (a) 1.12 mm, (b) 1.22 mm, (c) 1.26 mm, (d) 1.36 mm, (e) 1.41 mm, and (f) rupture. Scale bar, 1 mm.

4.3 Equivalent strain analysis

4.3.1 Assumptions

In order to obtain strain data of the material from SPCT, the equivalent strain analysis in Chakrabarty's membrane stretching theory [5] is applied since stress state of an SPCT specimen during deformation is not simple and, therefore, SPCT results are incompatible with results of conventional uniaxial creep test. In other words, raw data of SPCT results cannot be directly used to assess creep life of material in that punch displacement is not the same with strain. Hence, additional interpretation on SPCT results should be followed and, in this regard, Chakrabarty's membrane stretching theory is used in this paper. Before the equivalent strain analysis is carried out, two significant assumptions in Chakrabarty's membrane stretching theory should be discussed.

First, material is assumed to not only be isotropic, but also undergo pure plastic deformation explained in theory of plasticity [5]. Based on these assumptions, material shows incompressible characteristics and, therefore, plastic deformation equations such as the von-Mises equivalent strain are simplified. However, an SPCT specimen undergoes “creep” deformation not perfect plastic deformation. Nevertheless, it is reasonable that the equivalent strain analysis is used to interpret SPCT results since the above simple assumptions of plasticity theory hold reasonably even during steady state creep at high temperature unless there is metallurgical changes in material [29, 48, 49].

Also, Chakrabarty's membrane stretching theory does not consider friction effect between punch ball and specimen, while the SPCT, in reality, is affected by friction

force [28]. Besides, the author has suggested that only a few certain materials are suitable for the equivalent strain analysis. Although not only the perfect lubrication is not a real situation but also feasible materials are limited, the equivalent strain analysis is meaningful enough for a simple approximate solution. Moreover, outcomes resulted from the equivalent strain analysis are applied to the Monkman-Grant model in which an overall trend is more important than single data. In this regard, the whole SPCT results by Si_3N_4 and Al_2O_3 punch balls in Figure 4.3 are used to build the Monkman-Grant model and the effect of friction is also discussed.

4.3.2 Graphical method

The equivalent strain in equation 2.4.6 can be derived from the direct investigation of the least thickness change in an SPCT specimen. Substituting equation 4.2.1 into equation 2.4.6 yields the equivalent strain with respect to the punch displacement [45].

$$\varepsilon_q = 1.2(\frac{h}{2})^{1.5} \tag{4.3.1}$$

Since the equivalent strain is obtained directly from small punch test result by using equation 4.3.1, no more FE analysis is required to investigate stress and strain equivalent to uniaxial test results.

This direct analytical solution to small punch test can be also applied to SPCT because the main fracture occurs near the thinnest point and thickness change versus the punch displacement shows the similar trend in both tests although test condition and microscopic deformation mechanism are not exactly the same. Under this assumption, substitution of the displacement results of SPCT in Figure 4.3 into equation 4.3.1 yields the conversion of punch displacement into the equivalent strain ε_q. The equivalent strain rate $\dot{\varepsilon}_q$ can be also obtained simply by taking time derivative of the equivalent strain ε_q. Especially, MATLAB, commercial software, is used to acquire a time derivative between two consecutive data points. Hence, the proposed method enables us to investigate creep properties directly from SPCT without any aid of FE simulation and reference data from uniaxial creep test as shown in Figure 4.6 which is derived by applying 470.88 N with Si_3N_4 punch ball.

Note that there are lots of noises in Figure 4.6 (a) because creep test usually

takes long time and produces a plethora of data. In contrast, equivalent strain ε_q and rate $\dot{\varepsilon}_q$ curves in Figure 4.6 (b) and (c) look more stabilized by data filtering. Due to this reason, data filtering in creep test is generally allowed to procure constant minimum creep rate $\dot{\varepsilon}_s$ [12]. Thus, data filtering of SPCT is carried out and the results are shown in Appendix. Steady state region is determined in Figure 4.6 (c), and minimum equivalent strain rate $\dot{\varepsilon}_{q,min}$ is calculated by average value of $\dot{\varepsilon}_q$ in the steady state region in Figure 4.6 (a).

The minimum equivalent strain rate $\dot{\varepsilon}_{q,min}$ and the corresponding failure time t_f for all SPCT results [28] are listed in Table 4.1 and Table 4.2. Both tables show a similar trend to the standard uniaxial creep test such that the minimum equivalent strain rate $\dot{\varepsilon}_{q,min}$ is inversely proportional to failure time t_f. Besides, the friction effect of punch ball, which not only affects the minimum punch displacement rate $\dot{h}_{min}$ but also the minimum equivalent strain rate $\dot{\varepsilon}_{q,min}$, can be elucidated quantitatively. The bigger friction coefficient of Si_3N_4 punch ball in Table 4.1 causes the smaller minimum equivalent strain rate $\dot{\varepsilon}_{q,min}$ compared to the case of Al_2O_3 punch ball in Table 4.2 under the same loading condition. These results suggest that friction effect between punch ball and specimen should be also considered as an important factor in SPCT.

In Figure 4.6, the equivalent strain curve is divided into three parts, one is initial stage including large deformation, another is steady state region and the other is tertiary stage showing sudden increase of equivalent strain ε_q and final failure time t_f. The steady state region also provides minimum equivalent strain rate $\dot{\varepsilon}_{q,min}$. This information is indispensable to creep life evaluation with the Monkman-Grant model which will be discussed in the next section. All equivalent strain and strain rate curves for SPCT results in Figure 4.3 are shown in Figure 4.7 and Figure 4.8.

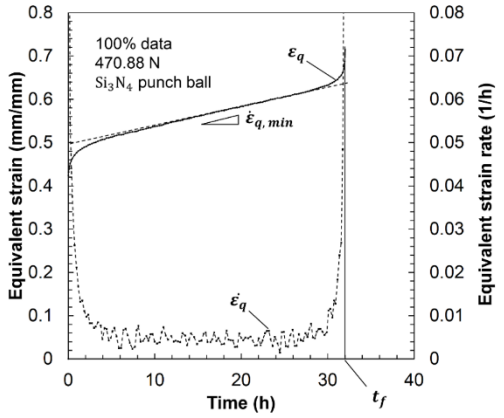

(a)

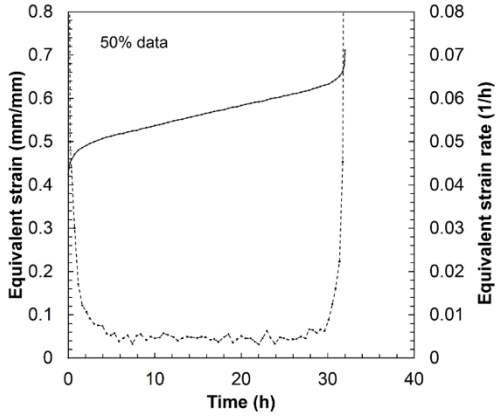

(b)

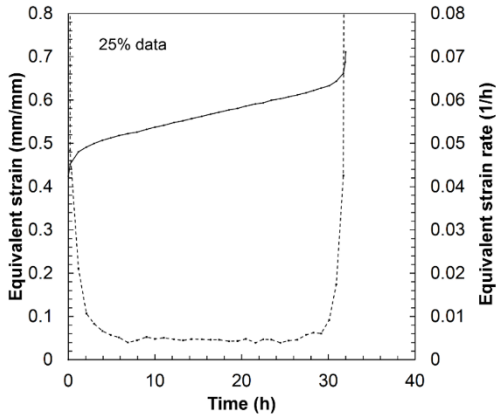

(c)

Figure 4.6 Equivalent strain and strain rate curves based on SPCT of STS 316L under 470.88 N with Si_3N_4 punch ball: (a) 100% data, (b) 50% data, and (c) 25% data

Table 4.1 Equivalent strain analysis results for SPCT using Si_3N_4 punch ball

Load (N)	Min. equivalent strain rate, $\dot{\varepsilon}_{q,min}$ (1/h)	Failure time, t_f (h)
421.83	0.0035	43.9
470.88	0.0043	32.0
549.36	0.0086	19.1
598.41	0.0172	15.0

Table 4.2 Equivalent strain analysis results for SPCT using Al_2O_3 punch ball

Load (N)	Min. equivalent strain rate, $\dot{\varepsilon}_{q,min}$ (1/h)	Failure time, t_f (h)
421.83	0.0045	33.1
470.88	0.0054	26.8
549.36	0.0090	17.4
598.41	0.0188	11.5

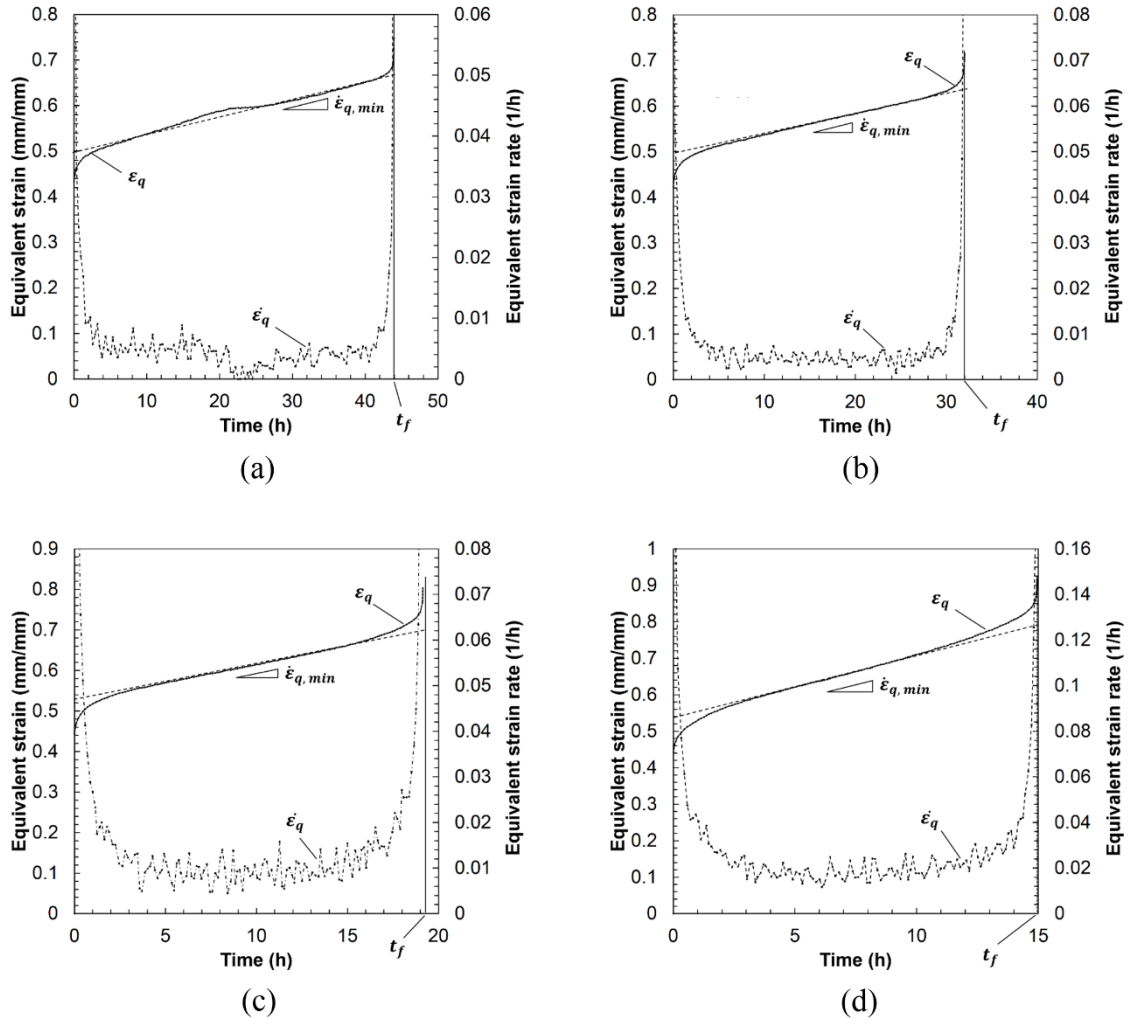

Figure 4.7 Equivalent strain and equivalent strain rate using Si_3N_4 punch ball for four different load conditions: (a) 421.83 N; (b) 470.88 N; (c) 549.36 N; and (d) 598.41 N

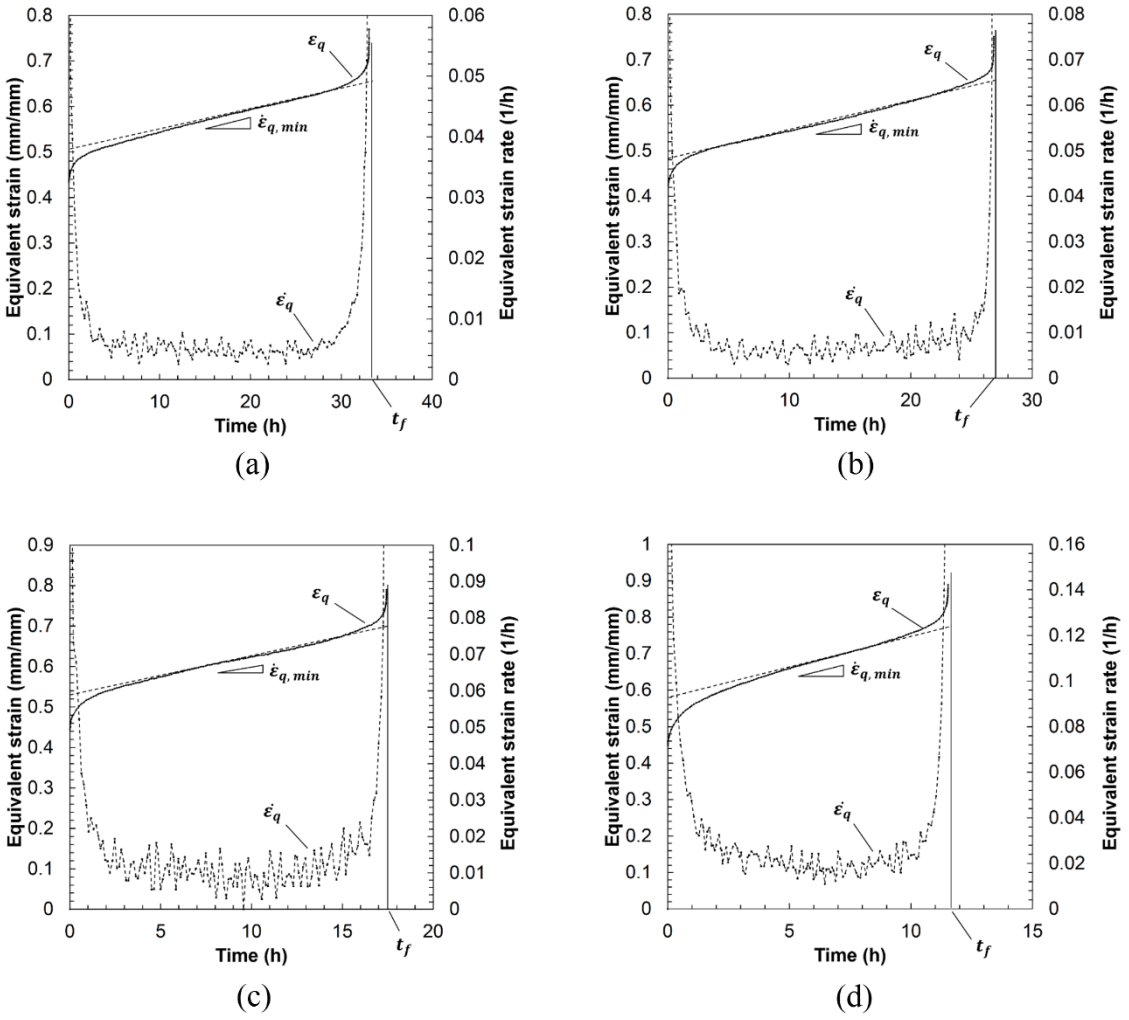

Figure 4.8 Equivalent strain and equivalent strain rate using Al_2O_3 punch ball for four different load conditions: (a) 421.83 N; (b) 470.88 N; (c) 549.36 N; and (d) 598.41 N

4.4 Derivation of Monkman-Grant model

The Monkman-Grant model in equation 2.5.1 is used to substantiate the equivalent strain analysis of SPCT results. From Figure 4.7 and 4.8, the minimum equivalent strain rate $\dot{\varepsilon}_{q,min}$ and failure time t_f can be obtained to make the Monkman-Grant model for SPCT.

For validation of the proposed direct methodology in this paper, Im's results [27] in which the uniaxial creep test for STS 316L has been carried out at 650℃ are also used to build the Monkman-Grant model. Im has conducted four different stress conditions which are 210, 230, 250, and 270 MPa. Creep properties of STS 316L at 650℃ such as minimum creep rate $\dot{\varepsilon}_s$, failure time t_f, and total strain to failure ε_f are also provided in Table 4.3. Especially, $\dot{\varepsilon}_s$ and t_f are used to make the Monkman-Grant model for the uniaxial creep test.

Table 4.3 Creep properties of STS 316L at 650℃ [27]

Stress (MPa)	ε_f	$\dot{\varepsilon}_s$ (1/h)	t_f (h)
210	0.4038	0.00029	205.2
230	0.2577	0.00201	67.8
250	0.3328	0.00613	27.0
270	0.2688	0.00843	18.4

Figure 4.9 shows three Monkman-Grant models, one is for the uniaxial creep test and others are for SPCT. Their parameters are summarized in Table 4.4. Since these three Monkman-Grant models show a close similarity to one another, the direct solution from the equivalent strain concept using the membrane stretching theory has

a strong potential for a novel and unique interpretation without any additional endeavor such as uniaxial creep test and FE analysis. Distribution of the Monkman-Grant model from SPCT and uniaxial creep test results also explains another advantage of SPCT which is shorter test time than uniaxial creep test. This is because SPCT results show faster minimum strain rate and shorter failure time than uniaxial creep test results.

And two different punch balls, which are Si_3N_4 and Al_2O_3, do not significantly affect the Monkman-Grant model for SPCT. Not only from comparing uniaxial creep test with SPCT but also comparing each SPCT result, there is little effect of friction coefficient of punch ball in the Monkman-Grant model. Therefore, creep life prediction using the Monkman-Grant model is independent in effect of punch ball.

Table 4.4 Parameters for Monkman-Grant model of each test type

Test type	*m*	*C*
Uniaxial creep test	0.700	0.738
SPCT (Si_3N_4 punch ball)	0.686	0.878
SPCT (Al_2O_3 punch ball)	0.784	0.513

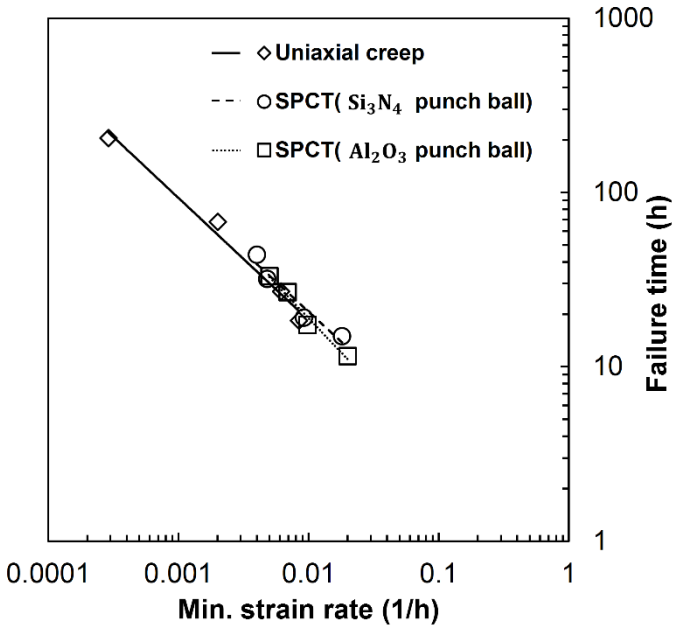

Figure 4.9 Comparison of the Monkman-Grant models of STS 316L for uniaxial creep test and SPCT with different punch balls at 650℃ [44]

5 Discussion

5.1 Overview of direct methodology

Figure 5.1 illustrates a direct procedure to obtain strain and strain rate only using SPCT. This flow chart provides a standard manual of SPCT for creep life estimation. Anyone can easily follow the flow chart step by step and, as a result, procure the Monkman-Grant model derived by SPCT.

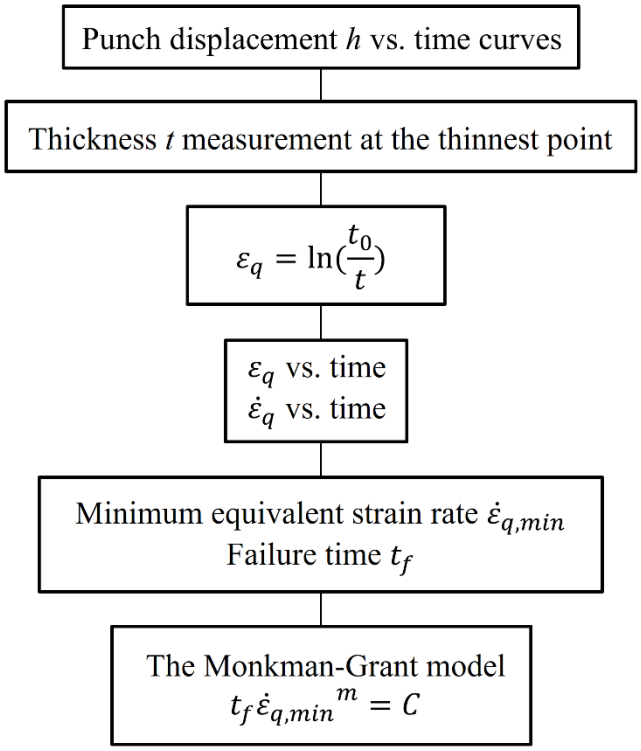

Figure 5.1 A flowchart of creep life prediction using SPCT [44]

First, an SPCT is carried out at elevated temperature using $10 \times 10 \times 0.5$ mm specimen to acquire a general SPCT curve which shows variation of punch displacement with respect to time. Based on the curve, interval to interrupt an SPCT is determined and, as following the interval, an SPCT is interrupted to measure thickness *t* at the thinnest point. How to measure the thickness *t* is explained in 3.3.3 thickness measurement section. The thickness change at the thinnest point is applied to the equivalent strain in equation 2.4.6, and then the equivalent strain rate $\dot{\varepsilon}_q$ is derived with respect to time. In the equivalent strain rate $\dot{\varepsilon}_q$ curve, the minimum equivalent strain rate $\dot{\varepsilon}_{q,min}$ should be calculated as average of $\dot{\varepsilon}_q$ on steady-state stage. As a result, the minimum equivalent strain rate $\dot{\varepsilon}_{q,min}$ and failure time t_f are obtained. Finally, the Monkman-Grant model can be drawn like Figure 4.9.

This direct methodology is very straightforward and practical. This is because the equivalent strain analysis can be applied to simple measurement of the least thickness on specimen, and therefore FE analysis is not needed to derive strain value.

Furthermore, the direct methodology is very useful since previous studies cannot be easily matched to other researchers' study due to difference of FE model. In other words, if FE model is different, FE analysis to derive strain value can yield different results even though material is same. For this reason, a correction factor, which is needed to compare SPCT with uniaxial creep test, is different as each study of SPCT and, therefore, referring to other outcomes is difficult. In this regard, the direct methodology will play a strong role to make SPCT results more compatible with others since the methodology needs no correction factor.

Besides, the direct methodology is robust and reasonable because a physical understanding on deformation of an SPCT specimen is underlain in the methodology. In a great deal of previous studies on SPCT, however, a correction factor is usually

used without understanding of mechanical deformation. In other words, the correction factor is a tool to adjust results rather than a fundamental solution. However, in this paper, understanding on deformation of SPCT specimen is firstly carried out and, thus, equivalent strain rate $\dot{\varepsilon}_q$ for SPCT is obtained analytically and graphically.

In conclusion, the direct methodology can make SPCT more practical. For further application, a real-time monitoring of creep life for in-service component can be realized. To fulfill it, not only a great deal of material should be used to validate the direct methodology, but also effect of temperature should be investigated.

5.2 Review of direct methodology-complementary investigation

5.2.1 Validation process

In this paper, Mao's result, equation 4.3.1 obtained by small punch test at room temperature, is used to derive the equivalent strain value. Although the outcome shown in Figure 4.9 is good, variation of the least thickness at high temperature must be investigated and substantiated whether there is difference between Mao's result and the variation of the least thickness at creep condition. To be specific, temperature and load dependency should be elucidated in the variation of the least thickness.

In this study, however, mechanical viewpoint rather than metallurgical viewpoint is strongly underlain to develop the direct methodology in which reasonable assumptions of plasticity theory exist. Based on these assumptions such as perfect plastic deformation, citation of Mao's result is acceptable even though it is an approximation.

Furthermore, a main objective of this paper is to suggest a possibility to overcome limitations in previous studies on SPCT. In this regard, the direct methodology is worthwhile enough.

As already mentioned above, a plethora of previous studies on SPCT have to use a correction factor in which physical meaning exists little, while no correction factor is needed in this study. However, no correction factor just might mean that a correction factor for STS 316L is 1 since only STS 316L is used to validate the direct methodology. For instance, the Monkman-Grant model by another material's SPCT result might not be similar with that by same material's uniaxial creep test. Additional investigation, therefore, should be carried out with various materials.

5.2.2 Metallurgical change

In this paper, metallurgical change in STS 316L at 650℃ for short test time is assumed to be little based on a reference [50], and therefore simple assumptions of plasticity theory can be applied to an SPCT specimen. However, various experiment conditions such as extremely high temperature, low load, and long test time are recommended to carry out since metallurgical change in STS 316L at these conditions is obvious [51]. In other words, equivalent strain analysis may be invalid because simple assumptions in theory of plasticity cannot be used if there is metallurgical change. This is a very sensitive issue in the direct methodology in that SPCT is not small punch test but small punch "creep" test at elevated temperature. Hence, a metallurgical investigation will play an important role to determine a feasible range in which the direct methodology is valid.

Furthermore, a metallurgical study is needed to carry out a real-time monitoring of creep life of in-service materials because the materials undergo aging at high temperature for long time and, thus, metallurgical change occurs. Therefore, the Monkman-Grant model derived by no aged material also can be affected. In this regard, investigation on how an aged material affects the Monkman-Grant model developed by the direct methodology would be highly meaningful for further practical use of the direct methodology.

6 Conclusion

Chakrabarty's membrane stretching theory is applied to obtain the equivalent strain from SPCT result. From this equivalent strain analysis, SPCT data, which is punch displacement and time, can be converted into strain and time. In order to compare results of SPCT with uniaxial creep test, creep properties and SPCT results of STS 316L are referred in this investigation. This comparison uses the Monkman-Grant model for uniaxial creep test and SPCT at same test temperature. As a result, each step in whole investigation is well explained and the step by step process is organized as a direct methodology for small punch creep test. Conclusions for this research are drawn.

(1) Chakrabarty's membrane stretching theory provides the equivalent strain data at the thinnest point even in the SPCT specimen. This can be obtained from investigation of thickness change at the thinnest point in the specimen and provides creep curve for SPCT.

(2) The Monkman-Grant model of SPCT result, which is obtained from the equivalent strain analysis, shows an excellent agreement with that of uniaxial creep test. Dispersion in the Monkman-Grant model of SPCT indicates faster minimum strain rate and shorter failure time than the uniaxial creep test and suggests SPCT can be substituted for uniaxial creep test. Hence, a real-time monitoring of in-service material's creep life is expected in the future.

(3) The Monkman-Grant models of SPCT from different punch balls, which are Si_3N_4 and Al_2O_3, show a similar trend with each other. This means that

effect of punch ball is not critical in the Monkman-Grant model of SPCT.

(4) In this paper, an empirical relation which is thickness change along punch displacement is used to apply the equivalent strain analysis. But, because this empirical relation is derived for small punch test not for small punch “creep” test, thickness measurement at the thinnest point of SPCT is, in the future, needed for more concrete validation of the direct solution.

(5) The used material for validation in this study is only STS 316L, and therefore additional investigation using various materials is also needed for more concrete validation. Furthermore, experimental conditions such as temperature, load, and test time should be considered likewise since these conditions can yield metallurgical change in the material.

References

1. Nobuo Tanaka, Roger Wicks (2010) power generation from coal. IEA. https://www.iea.org/publications/freepublications/publication/power_generation_from_coal.pdf. Accessed October 2010

2. American Society for Test and Materials (2006) ASTM E139-11: standard test methods for conducting creep, creep-rupture, and stress-rupture tests of metallic materials, book of standards, volume: 03.01

3. Parker, J.D., James, J.D. (1993) Disc-bend creep deformation behaviour of 0.5Cr0.5Mo0.25V low alloy steel. 5th International Conference on Creep and Fracture of Engineering Materials and Structures: 651-660.

4. Manahan, M.P. (1983) A new postirradiation mechanical behavior test—the miniaturized disk bend test. Nucl Technol 63:295-315.

5. Chakrabarty, J. (1970) A theory of stretch forming over hemispherical punch heads. Int J Mech Sci 12(4):315-325.

6. Yang, Z., Wang, Z.W. (2003) Relationship between strain and central deflection in small punch creep specimens. Int J Press Vessel Pip 80(6):397-404.

7. Chen, J., Ma, Y.W., Yoon, K.B. (2010) Finite element study for determination of material's creep parameters from small punch test. J Mech Sci Technol 24(6):1195-1201.

8. Hyde, T.H., Stoyanov, M., Sun, W., Hyde, C.J. (2010) On the interpretation of results from small punch creep tests. J Strain Anal Eng 45(3):141-164.

9. CEN/WS (2005) Small Punch Test Method for Metallic Materials Part 1: A Code of Practice for Small Punch Testing at Elevated Temperatures. Report No. CEN/WS 21

10. Milička, K., Dobeš, F. (2006) Small punch testing of P91 steel. Int J Press Vessel Pip 83:625-634.

11. Li, Y., Šturm, R. (2008) Determination of creep properties from small punch test. In: Proceedings of ASME pressure vessels and piping division conference, Chicago, Illinois, pp 739-750

12. Alegre, J.M., Cuesta, I.I., Lorenzo, M. (2014) An Extension of the Monkman-Grant Model for the Prediction of the Creep Rupture Time Using Small Punch Tests. Exp Mech 54:1441-1451.

13. Zhai, P.C., Chen, G., Hashida, T., Zhang, Q.J. (2005) Evaluation on small punch creep test by finite element method. Key Eng Mat 297-300:377-383.

14. Ling, X., Zheng, Y., You, Y., Chen, Y. (2007) Creep damage in small punch creep specimens of Type 304 stainless steel. Int J Press Vessel Pip 84:304-309.

15. Evans, M., Wang, D. (2008) The small punch creep test: Some results from a numerical model. J Mater Sci 43:1825-1835.

16. Ma, Y.W., Shim, S., Yoon, K.B. (2009) Assessment of power law creep constants of Gr91 steel using small punch creep tests. Fatigue Fract Eng M 32:951-960.

17. Park, T.G., Shim, S.H., Yoon, K.B., Jang, C.H. (2002) A study on parameters measured during small punch creep testing. Trans Korean Soc Mech Eng A 26(1):171-178 (in Korean with English Abstract).

18. Lee, Jong Hoon, et al. (2014) Analysis of the small punch creep test results according to the normalized lifetime fraction. Met Mater Int 20(5):835-839.

19. Dymáček, P., Milička, K. (2009) Creep small-punch testing and its numerical simulations. Mater Sci and Eng A 510–511:444-449.

20. Monkman, F.C., Grant, N.J. (1956) An empirical relationship between rupture life and minimum creep rate in creep-rupture tests. In proc. ASTM 56:593-620.

21. Ule, Boris, et al. (1999) Small punch test method assessment for the determination of the residual creep life of service exposed components: outcomes from an interlaboratory exercise. Nucl Eng Des 192(1):1-11.

22. Dobeš, F., Milička, K., Kratochvíl, P. (2004) Small punch creep in Fe28Al3Cr0. 02Ce alloy. Intermetallics 12(12):1397-1401.

23. Kim, B., Lim, B., Ki, D. (2006) Creep Behavior and Life Evaluation of Aged P92 Steel. Int J Mod Phys B 20(25n27):4231-4236.

24. Hou, F., Xu, H., Wang, Y., Zhang, L. (2013) Determination of creep property of 1.25 Cr0. 5Mo pearlitic steels by small punch test. Eng Fail Anal 28:215-221.

25. Mathew, M.D., Kumar, J.G., Ganesan, V., Laha, K. (2014) Small punch creep studies for optimization of nitrogen content in 316LN SS for enhanced creep resistance. Metall Mater Trans A 45(2):731-737.

26. Dobeš, F., Milička, K. (2002) On the Monkman–Grant relation for small punch test data. Mater Sci Eng A 336(1):245-248.

27. Im, J.W. (1998) The effect of prior aging on the creep rupture behavior of STS 316. Master thesis, Sungkyunkwan University, Seoul, Korea (in Korean with English Abstract).

28. Kim, B.J., Cho, N.H., Kim, M.K., Lim, B.S. (2011) Effect of friction coefficient on the small punch creep behavior of AISI 316L stainless steel. Korean J Met Mater 49:515-521 (in Korean with English Abstract).

29. Dieter, G.E., Bacon, D. (1986) Mechanical metallurgy (Vol. 3). New York: McGraw-Hill.

30. Robinson, S.L., Sherby, O.D. (1969) Mechanical behavior of polycrystalline tungsten at elevated temperature. Acta Metall Mater 17(2):109-125.

31. Ashby, M.F. (1972) A first report on deformation-mechanism maps. Acta Metall Mater 20(7):887-897.

32. Frost, H.J., Ashby, M.F. (1982) Deformation mechanism maps: the plasticity and creep of metals and ceramics. Pergamon Press, Oxford, UK.

33. Shen, Y.L., Suresh, S. (1996) Steady-state creep of metal-ceramic multilayered materials. Acta mater 44(4):1337-1348.

34. Nabarro, F.R. (1948) Report of a Conference on the Strength of Solids. The Physical Society, London, 75.

35. Herring, C. (1950) Diffusional viscosity of a polycrystalline solid. J Appl Phys 21(5):437-445.

36. Coble, R.L. (1963) A model for boundary diffusion controlled creep in polycrystalline materials. J Appl Phys 34:1679.

37. Onaka, S., Huang, J.H., Wakashima, K., Mori, T. (1998) Kinetics of stress relaxation caused by the combination of interfacial sliding and diffusion: two-dimensional analysis. Acta mater 46(11):3821-3828.

38. Harper, J., Dorn, J.E. (1957) Viscous creep of aluminum near its melting temperature. Acta Metall Mater 5(11):654-665.

39. Harper, J.G., Shepard, L.A., Dorn, J.E. (1958) Creep of aluminum under extremely small stresses. Acta Metall Mater 6(7):509-518.

40. Chakrabarty, J. (2010) Applied plasticity, second edition. Springer, New York

41. Dunand, D.C., Han, B.Q., Jansen, A.M. (1999) Monkman-grant analysis of creep fracture in dispersion-strengthened and particulate-reinforced aluminum. Metall Mater Trans A 30:829-838.

42. Outokumpu Stainless, A. B. (2013) Handbook of Stainless Steel. Avesta: Outokumpu Stainless AB.

43. Davis, J.R. (Ed.). (1994) Stainless steels. ASM international.

44. Lee, T., Ibupoto, F.A., Lee, J.H., Kim, B.J., Kim, M.K. (2015) A Direct Methodology for Small Punch Creep Test. Exp Mech 1-11.

45. Mao, X., Shoji, T., Takahashi, H. (1987) Characterization of fracture behavior in small punch test by combined recrystallization-etch method and rigid plastic analysis. J Test Eval 15:30-37.

46. Cuesta, I.I., Alegre, J.M., Lacalle, R. (2010) Determination of the Gurson–Tvergaard damage model parameters for simulating small punch tests. Fatigue Fract Eng M 33(11):703-713.

47. Chakrabarty, J. (1998) Large deflections of a clamped circular plate pressed by a hemispherical-headed punch. Met Mater Int 4(4):680-684.

48. Soderberg, C.R. (1936) The interpretation of creep tests for machine design. Trans. ASME, 58(8).

49. Johnson, A.E. (1960) Complex-stress creep of metals. Metallurgical Reviews, 5(1):447-506.

50. Minami, Y., Kimura, H., Ihara, Y. (1986) Microstructural changes in austenitic stainless steels during long-term aging. Materials science and technology 2(8):795-806.

51. Weiss, B., Stickler, R. (1972) Phase instabilities during high temperature exposure of 316 austenitic stainless steel. Metall Trans 3(4):851-866.

Appendix

1. Equivalent strain analysis results and data sampling

Equivalent strain analysis yields general creep diagram in which important creep properties can be procured directly. However, creep test including SPCT generates a plethora of data and, therefore, data sampling is needed to better understand creep properties of materials. Figure A1 to A7 show effect of data sampling with respect to 100%, 50%, and 25% data. From this additional work, equivalent strain rate line becomes much smoother. Figure A1 to A3 are derived by SPCT of STS 316L with Si_3N_4 punch ball [28] and each figure means different load conditions as 421.83, 549.36, and 598.41 N, respectively. Likewise, Figure A4 to A7 are illustrated by SPCT of STS 316L with Al_2O_3 punch ball [28] and each figure means different load conditions as 421.83, 470.88, 549.36, and 598.41 N, respectively.

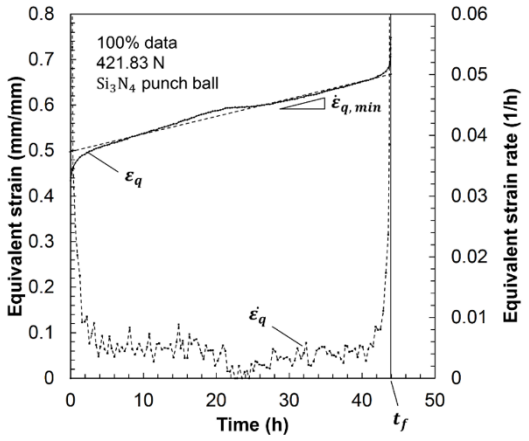

(a)

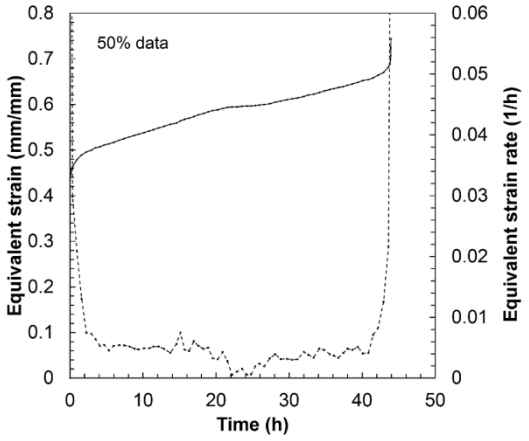

(b)

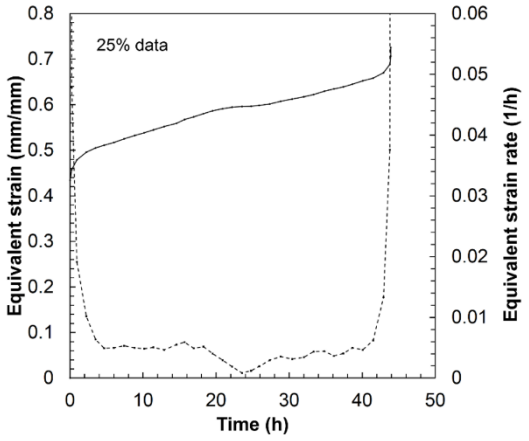

(c)

Figure A1 Equivalent strain and strain rate curves under 421.83 N with Si_3N_4 punch ball: (a) 100% raw data, (b) sampling by 50%, and (c) sampling by 25%

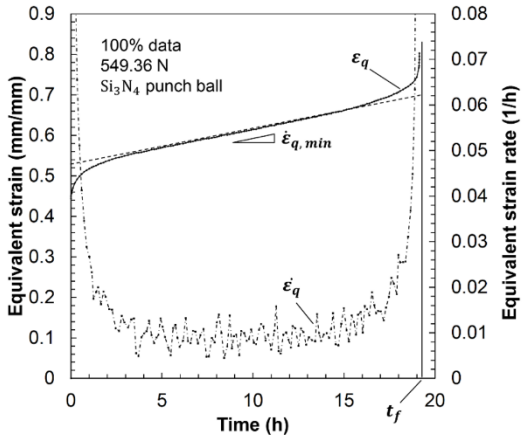

(a)

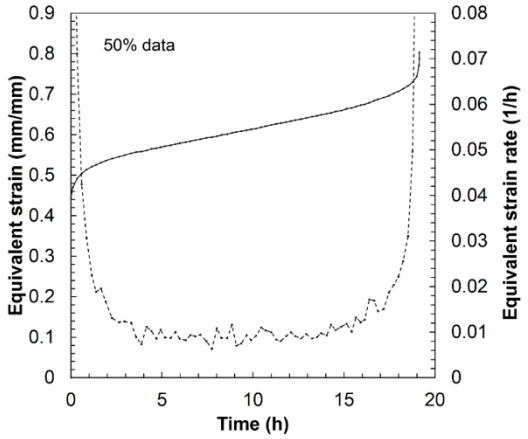

(b)

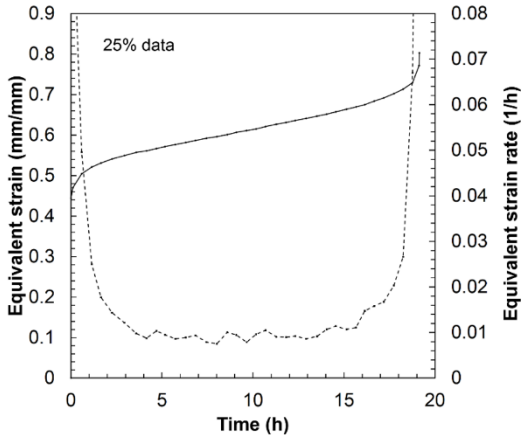

(c)

Figure A2 Equivalent strain and strain rate curves under 549.36 N with Si_3N_4 punch ball: (a) 100% raw data, (b) sampling by 50%, and (c) sampling by 25%

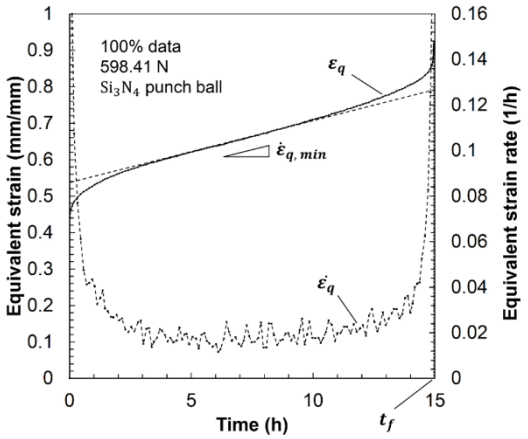

(a)

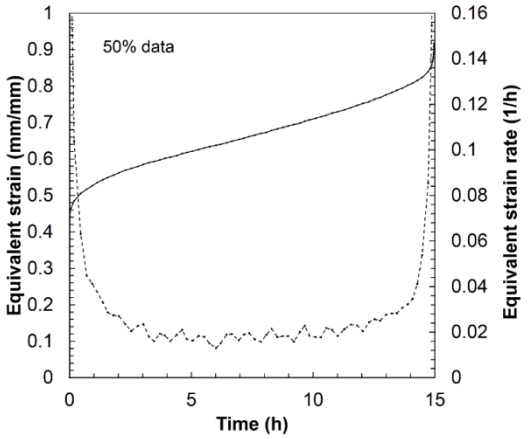

(b)

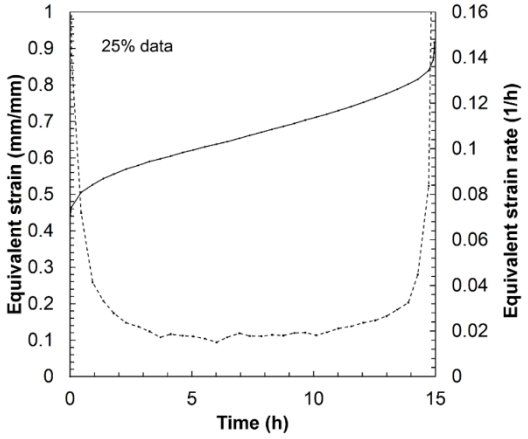

(c)

Figure A3 Equivalent strain and strain rate curves under 598.41 N with Si_3N_4 punch ball: (a) 100% raw data, (b) sampling by 50%, and (c) sampling by 25%

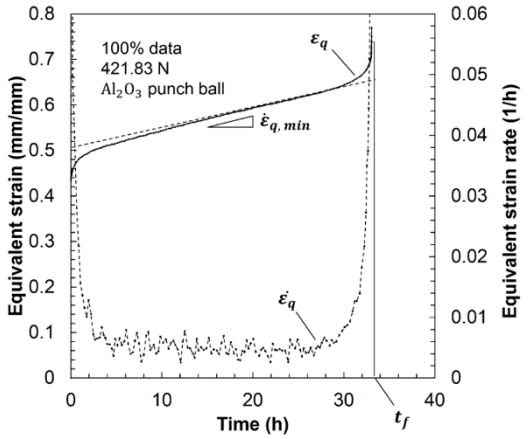

(a)

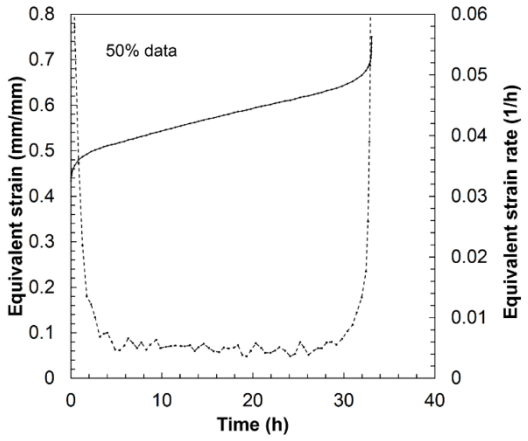

(b)

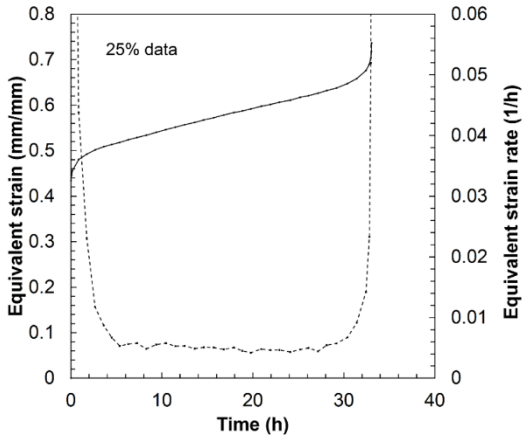

(c)

Figure A4 Equivalent strain and strain rate curves under 421.83 N with Al_2O_3 punch ball: (a) 100% raw data, (b) sampling by 50%, and (c) sampling by 25%

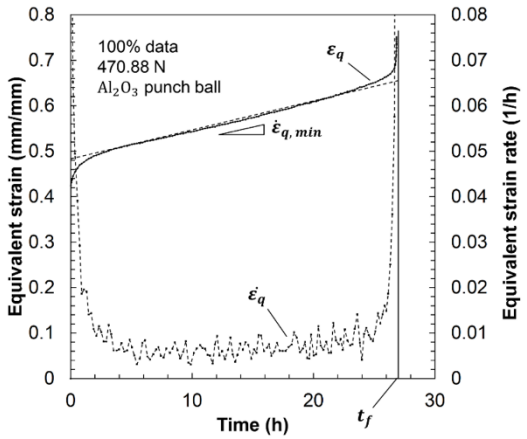

(a)

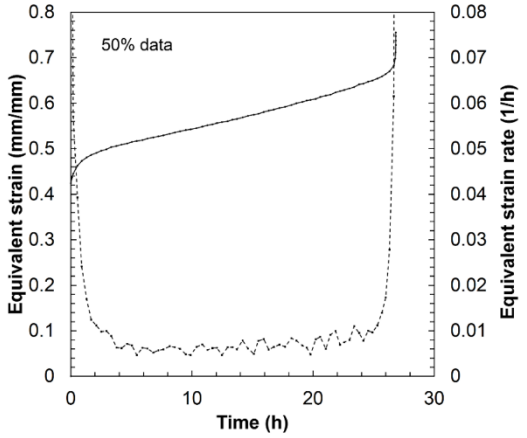

(b)

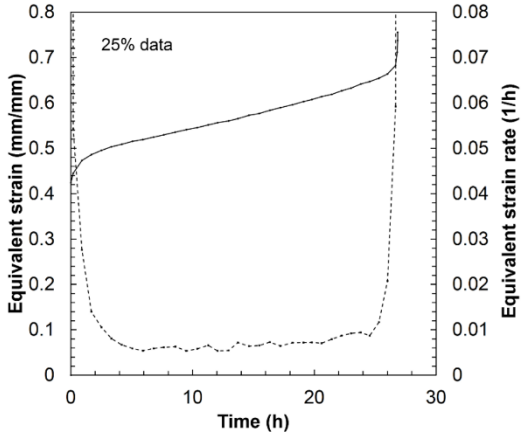

(c)

Figure A5 Equivalent strain and strain rate curves under 470.88 N with Al_2O_3 punch ball: (a) 100% raw data, (b) sampling by 50%, and (c) sampling by 25%

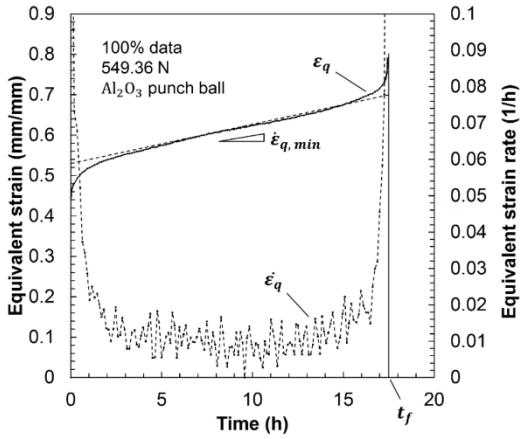

(a)

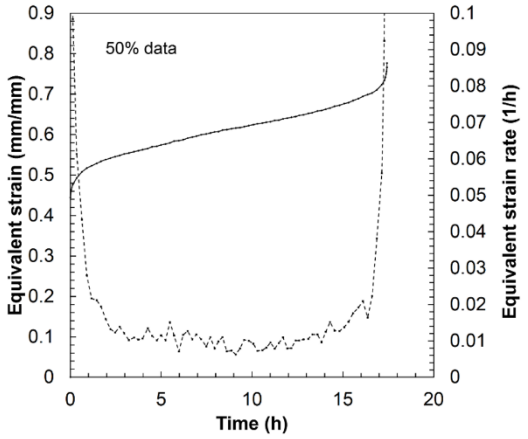

(b)

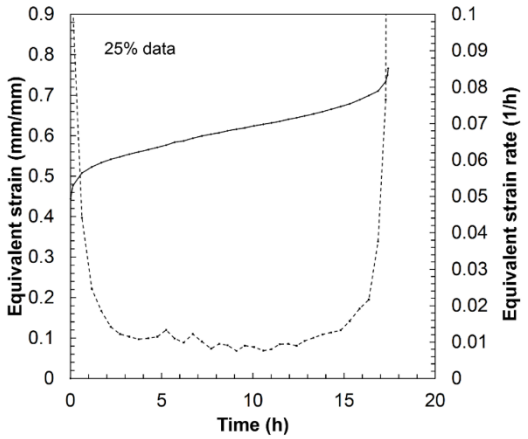

(c)

Figure A6 Equivalent strain and strain rate curves under 549.36 N with Al_2O_3 punch ball: (a) 100% raw data, (b) sampling by 50%, and (c) sampling by 25%

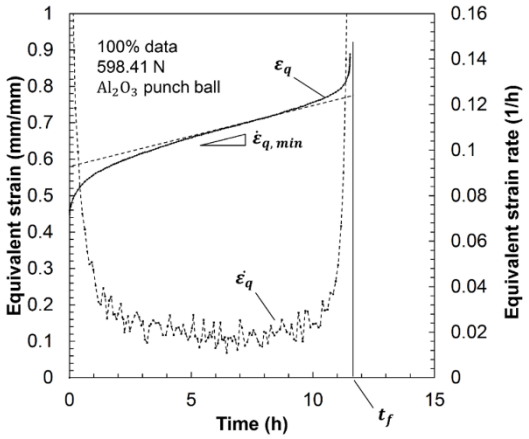

(a)

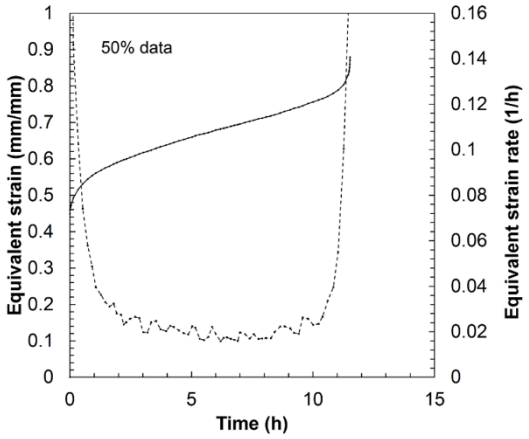

(b)

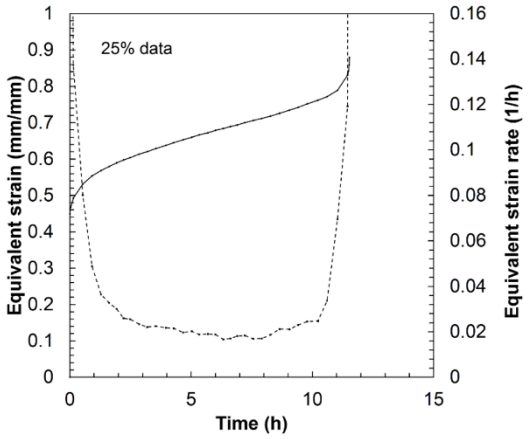

(c)

Figure A7 Equivalent strain and strain rate curves under 598.41 N with Al_2O_3 punch ball: (a) 100% raw data, (b) sampling by 50%, and (c) sampling by 25%

Abstract

소형 펀치 크리프 시험법에 기반한 크리프 수명 예측의 직접적 방법론 연구

성균관대학교 기계공학과

이 택 상

소형 펀치 크리프 시험법은 손톱만 한 크기($10 \times 10 \times 0.5$ mm)의 시편만으로 재료의 크리프 물성을 평가할 수 있는 잠재력이 있는 차세대 크리프 시험법이다. 작은 크기의 시편이란 장점으로 현재 운용 중인 발전소 설비에서 직접 시편을 채취하여 실시간으로 크리프 물성을 모니터링할 수 있다는 가능성을 가지고 있다. 하지만 소형 펀치 크리프 시험법은 시편 변형이 다축 응력 상태 하에서 발생하므로 기존 일축 크리프 시험법의 결과와 직접적으로 비교하는 것이 불가하다. 소형 펀치 크리프 시험법의 물리량은 하중(N)과 펀치 변위(mm)인 반면, 일축 크리프 시험법의 물리량은 응력(N/m^2)과 변형률(mm/mm)이다. 두 크리프 시험법의 물리량 차이를 극복하기 위해서는 소형 펀치 크리프 시편의 변형 메커니즘에 대한 이해가 선행되어야 하는데, 본 논문에서는 박막 스트레칭 이론을 적용하여 소형 펀치 크리프 시편의 변형 메커니즘을 분석하였다. 이에 따라 소형 펀치 크리프 시편의 유효변형률은 두께 방향의 진변형률의 크기로 단순화가 되며 시편의 가장 얇은 부분인 파단 부위의 두께 측정을 통해 유효변형률을 도출할 수 있다. 이 결과는 몬크만 그랜트 모델(Monkman-Grant model)에 적용되며 장시간 크리프 수명 예측을 위해 사용될 수 있다. 이를 실증하기 위해서 STS 316L의 일축 크리

프 실험 결과와 소형 펀치 크리프 실험 결과가 함께 인용되며 몬크만 그랜트 선도에서 상호 비교된다. 같은 재료와 온도에서 수행된 일축 크리프 실험과 소형 펀치 크리프 실험의 몬크만 그랜트 모델은 서로 상당히 유사하게 나타나는 것을 확인하였으며, 이를 통해 박막 스트레칭 이론을 적용한 유효 변형률 분석이 소형 펀치 크리프 시험법에 유효하다는 것도 확인할 수 있었다. 또한, 소형 펀치 크리프 실험만으로 몬크만 그랜트 모델을 만들 수 있고 단시간 크리프 수명 영역을 통해 외삽법을 이용한 장시간 크리프 수명 예측 역시 가능하다는 것을 확인하였다.

주제어: 소형 펀치 크리프 시험법, 박막 스트레칭 이론, 몬크만 그랜트 모델 (Monkman-Grant model), STS 316L